FEATURE ARTICLE

Exposing Solvent's Roles in Electron Transfer Reactions: Tunneling Pathway and Solvation

M. B. Zimmt*

Chemistry Department, Brown University, Providence, Rhode Island 02912

D. H. Waldeck*

Chemistry Department, University of Pittsburgh, Pittsburgh, Pennsylvania 15260

Received: October 14, 2002; In Final Form: March 3, 2003

We describe studies of electron transfer in donor−spacer−acceptor molecules for which the highly curved spacer topology imparts a vacant cleft along the "line-of-sight" between the electron donor and electron acceptor moieties. The electron transfer kinetics in nondipolar and weakly polar solvents allow experimental determination of the reaction free energy as a function of solvent structure and temperature. These data were used to parametrize a molecular solvation model developed by Matyushov. The model provides reasonable estimates of reaction free energy in solvents that are too polar for its direct measurement and provides reasonable values of the solvent reorganization energy in all solvents. Successful modeling of the solvation enables quantitative study of the factors that control electron tunneling through molecules located in the solute's cleft, i.e., the electronic coupling. Electron tunneling in these systems is mediated by the unoccupied orbitals of the solvent ("electron-mediated superexchange"). The solvent molecule's presence within the cleft is critical for effective electronic coupling, and its motion modulates the electronic coupling magnitude. These studies demonstrate and quantify the importance of electron tunneling "pathways" through noncovalent contacts for this model system and indicate that such pathways can contribute significantly to electron-transfer processes in biological and chemical systems.

Introduction

Electron transfer reactions constitute a fundamental chemical process and are of intrinsic importance in biology, chemistry, and emerging fields of nanotechnology. Biological processes such as photosynthesis and respiration rely on electron transfer between molecular subsystems that interact through a collection of covalent and noncovalent linkages. Electron tunneling in nanometer scale systems depends on similar interactions. Control of device properties will improve through a better understanding of the fundamental interactions that govern electron tunneling probabilities.

Electron transfer reactions differ from conventional chemical transformations in a number of substantive ways. The formation or rupture of covalent bond(s) between the reactants is not required for electron transfer reactions. In addition, the canonical reaction constraint, reactants in van der Waals contact, is relaxed for electron transfer processes, resulting in elementary electron transfer steps at reactant separations as large as tens of angstroms. The occurrence of electron transfer over a range of reactant separations and orientations complicates the interpretation of the transfer dynamics between freely diffusing donors and acceptors, because reactant diffusion and the intrinsic electron transfer process jointly determine the kinetics. Covalently linking the electron donor and acceptor units, creating a supermolecule with a single conformation, eliminates the influences of diffusion and multiple transfer distances and enables elucidation of the factors that determine the activation free energy and the preexponential factor in the rate expression for electron transfer.[1] Use of covalent spacers provides structural control, allowing investigation of the influence of donor−acceptor separation,[2] orientation,[3] stereochemistry,[3b,4] and spacer composition[5] on electron transfer rate constants. The topology of most supramolecular electron transfer molecules locates the spacer on the "line-of-sight" between the donor and the acceptor (Scheme 1). This design excludes solvent from the region directly between the donor and acceptor and the covalent linkages of the spacer mediate the electronic coupling.

Our groups and others have studied donor−spacer−acceptor supermolecules with topologies that permit solvent or appended groups in the space directly between the donor and acceptor (Scheme 1). These supermolecules contain highly curved spacers that extend from the donor and acceptor in directions orthogonal to their 'line-of-sight'. Kinetic studies identify two primary roles for solvent in promoting electron transfer reactions in these highly curved supermolecules. First, the differential solvation of the reactant and product states determines the free energy and the reorganization energy for the reaction. Our studies have used a molecular solvation model to describe these parameters, for both dipolar and nondipolar solvents. Second, the solvent molecules modulate the donor−acceptor electronic coupling; the electron tunneling occurs by way of solvent molecule orbitals. This phenomenon is not found for the linear donor−

* To whom correspondence should be addressed.

10.1021/jp022213b CCC: $25.00
Published on Web 04/23/2003

SCHEME 1: Molecular Structures for Different Donor−Spacer−Acceptor Molecules

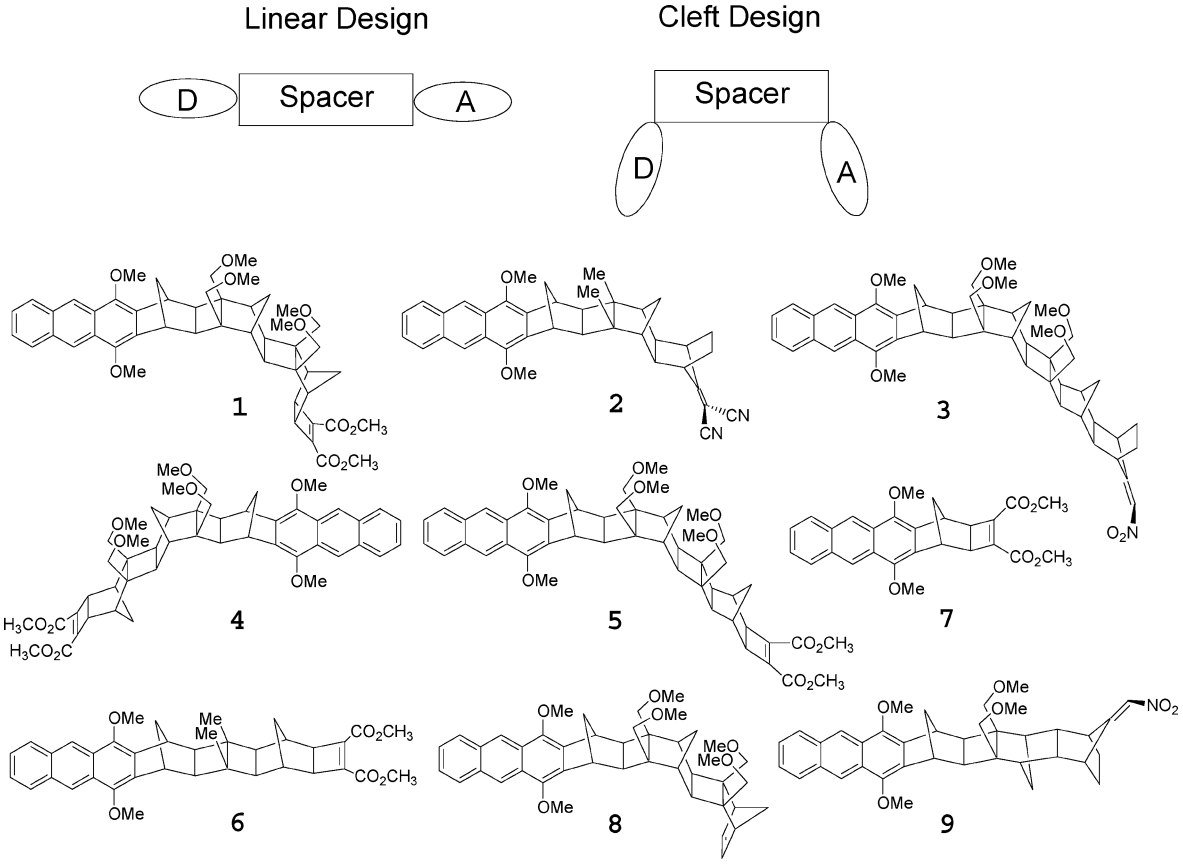

spacer−acceptor structures but has a dramatic influence on electron-transfer rate constants in curved spacer systems, a factor of ten and more, and is likely to find important analogues in biological and bimolecular electron transfers.

The rest of this article consists of four principal sections that summarize our investigations of solvent-mediated coupling. The first section provides background on the mechanistic model for electron transfer in donor−spacer−acceptor molecules and describes the experimental approach and system characterization used in our recent work. The next section describes the important considerations in understanding solvation in these systems and its quantitative modeling. The section that follows discusses the experimental evidence for and the characterization of the solvent's role in mediating electron tunneling. The last section summarizes the current status of this field and identifies some interesting avenues for future work.

Background

Electron transfer reactions are typically classified as occurring in one of two limits: the strong electronic coupling or adiabatic charge-transfer regime (where the rate constant is solvent friction dependent) and the weak electronic coupling or nonadiabatic regime (where the rate constant is distance dependent and solvent friction independent).[6] Figure 1 uses a simple one-dimensional reaction coordinate to illustrate how the electron transfer mechanism differs in these two regimes. The solid curve illustrates the adiabatic regime, in which the system's electronic state adiabatically follows the nuclear displacement, and the rate-limiting event for the reaction is the evolution of the system along the nuclear coordinate and through the transition state. The dashed curves in the figure correspond to the diabatic

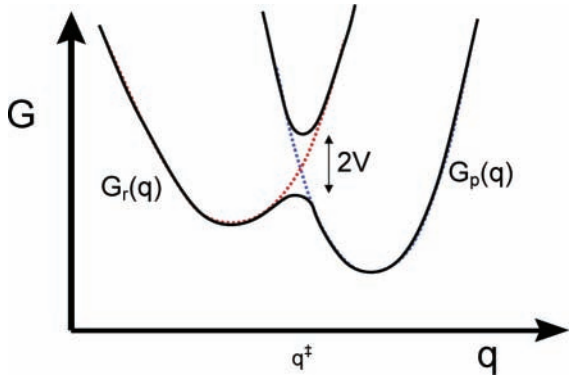

Figure 1. Diagram illustrating the two pictures (adiabatic and nonadiabatic) for the electron transfer.

reactant and product electronic states. In the nonadiabatic limit, the system moves through the transition state region (crossing point of the curves) many times before the electronic state switches from the diabatic reactant surface to the diabatic product curve; that is, the rate-limiting factor depends on the probability of hopping from one electronic surface to the other rather than just the probability of reaching the transition state through nuclear motion. The electron-transfer reactions of the donor-spacer-acceptor molecules in Scheme 1 fall within the nonadiabatic regime.

In the nonadiabatic limit, the rate constant k_{et} is written as

$$k_{et} = \frac{2\pi}{\hbar}|V|^2\mathrm{FCWDS} \qquad (1)$$

This equation has two elements: (1) the Franck−Condon factor (FCWDS) which depends on structural and environmental

variables and (2) the electronic coupling ($|V|$) which depends on the electronic properties of the medium between the electron donor and acceptor groups. The FCWDS term (eq 1) accounts for the probability that the system achieves a nuclear configuration in which the diabatic electronic states cross. Importantly, this formulation assumes that the electronic coupling is independent of the nuclear coordinate. In 1976, Jortner[7] used this Golden Rule formula to derive an expression for the FCWDS that accounted for both quantum mechanical and classical nuclear degrees of freedom. In the general case, this term can be written as

$$\mathrm{FCWDS} = \frac{\left[\sum_i \sum_f \exp(-E_i/kT)|\langle \mathrm{i}|\mathrm{f}\rangle|^2 \delta(E_i - E_f)\right]}{\left[\sum_i \exp(-E_i/kT)\right]} \quad (2)$$

where E_i is the energy of vibronic state i, E_f is the energy of vibronic state f, and $\langle i|f\rangle$ is their overlap. The sums are performed over all initial vibronic states i and over all final vibronic states f. This expression represents a thermally averaged value for the Franck−Condon overlap between the initial and final vibronic states. Frequently systems are modeled as possessing two sets of vibronic modes: one set that is very low frequency ($\nu < kT/h$) and modeled classically and a second set that is higher frequency ($\nu \gg kT/h$) and treated quantum mechanically. Contributions to the FCWDS from the classical degrees of freedom are included through the outer sphere reorganization energy λ_o, whereas the quantum degrees of freedom are included through a product of effective harmonic modes i with quantum number n_i and frequencies ν_i. The change in energy (reorganization) for each quantum degree of freedom is given by λ_i. Detailed investigations of the vibrational state dependence of the electron-transfer dynamics are few, but those available are consistent with this model.[8]

In the analysis of rate constants, there is generally insufficient vibrational information to model all of the quantized modes. In these cases, a coarser representation of the quantized modes is used. With only one quantum mode,[1c] the rate constant expression becomes

$$k_{et} = \frac{4\pi^2}{h}|V|^2 \frac{1}{\sqrt{4\lambda_o \pi k_B T}} \sum_{n=0}^{\infty} \exp(-S)\left(\frac{S^n}{n!}\right) \times \exp\left[-\frac{(\Delta_r G + \lambda_o + nh\nu)^2}{4\lambda_o k_B T}\right] \quad (3)$$

where ν is an effective frequency for the quantized vibrational mode, $\Delta_r G$ is the reaction free energy, S is the Huang−Rhys factor $\lambda_v/h\nu$, and λ_v is the total inner sphere reorganization energy for all of the relevant modes. The summand n refers to the product's vibrational quantum levels. For the systems studied below, the first few terms in the sum over product vibrational states provide an accurate evaluation of the rate constant, and eq 3 affords a reasonable description of the rate constant.

The primary aim of the studies described herein has been to evaluate the electronic coupling between a donor and acceptor that is mediated by nonbonded contacts with solvent molecules. The donor−spacer−acceptor molecules shown in Scheme 1 were investigated. Compound **1** has received the most attention because its cleft is of an appropriate size and shape to accommodate a single solvent molecule, and it exhibits equilibrium between the locally excited and charge separated state

SCHEME 2: Kinetic Scheme for the Forward and Back Electron Transfer

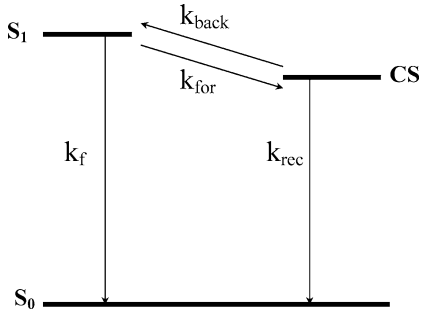

in many solvents. Compounds **2** and **3** have similar shapes as **1** but have different acceptor groups, with correspondingly distinct reaction free energies and larger donor-to-acceptor separations. Compounds **4** and **5** have the same topology, donor, and acceptor group as **1** but greater charge-transfer distances.

The experimental studies rely on time-resolved fluorescence to monitor the kinetics of charge separation. A picosecond laser pulse excites the anthracene moiety (donor unit) to the S_1 state (also referred to as the locally excited state, LE), from which it decays by electron transfer to the acceptor unit, radiative emission, and nonradiative relaxation. The fluorescence studies provide the time decay characteristics of the initially excited state (the reactant) but do not directly detect the charge-separated state.[9] In polar solvents, the fluorescence decay of the anthracene moiety is a single exponential with a rate constant $k_{obs} = k_f + k_{et}$, where k_f is the decay rate of a control molecule that has the donor group attached to the spacer but no acceptor (**8**, Scheme 1) and k_{et} is the electron transfer rate constant. Energy transfer from the excited donor to the acceptor is highly endoergic. Thus, $k_{obs} - k_f$ may be assigned to electron transfer. In nondipolar solvents, the anthracene fluorescence decay is double exponential. Nondipolar solvents do not solvate the charge separated state of **1** as greatly as polar solvents. Consequently, the free energy of charge separation is close to zero and the locally excited and charge-separated states interconvert, leading to double exponential kinetics (see Scheme 2). Both the forward ($S_1 \rightarrow$ CS) and back (CS$\rightarrow S_1$) transfer rate constants, k_{for} and k_{back}, are obtained from the fluorescence data.[10]

The double exponential kinetics observed in weakly polar solvents are important as they enable determination of the reaction free energy, $\Delta_r G$.[11,12] Solving the differential equation for the kinetics, one finds that the fluorescence intensity should have the form

$$I(t) = a_+ \exp(-k_+ t) + (1 - a_+) \exp(-k_- t) \quad (4)$$

The primary rate constants in the kinetic scheme are obtained from the parameters in this expression, namely

$$k_{for} = a_+(k_+ - k_-) + k_- - k_f \quad (5)$$

for the forward rate constant

$$k_{back} = \frac{(k_+ - k_-)^2 - [(k_f + k_{for}) - (k_{back} + k_{rec})]^2}{4k_{for}} \quad (6)$$

for the backward rate constant, and

$$k_{rec} = k_+ + k_- - k_f - k_{for} - k_{back} \quad (7)$$

for the recombination from the charge separated state to the

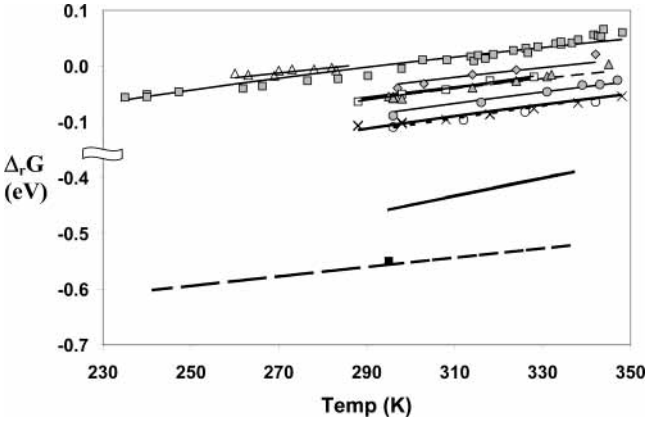

Figure 2. Experimental (symbols) and molecular model predicted (lines) values of the reaction free energy for charge separation, $\Delta_r G$ as a function of temperature. For clarity, the *y* axis has been broken at −0.15 eV. The solvents are 1,3,5-triisopropylbenzene (△), 1,3-diisopropylbenzene (shaded square), mesitylene (shaded diamond), 1,2,4-trimethylbenzene (□), cumene (shaded triangle), toluene (shaded circles), 2,5-dichlorotoluene (×), benzene (○), and acetonitrile (■). The line through the data points for each solvent corresponds to the molecular model predictions. The line with zero associated data points is the molecular model prediction for chlorobenzene. The long dashed line is the molecular model prediction for acetonitrile; the short dash line is for benzene; and the intermediate dash line is for cumene.

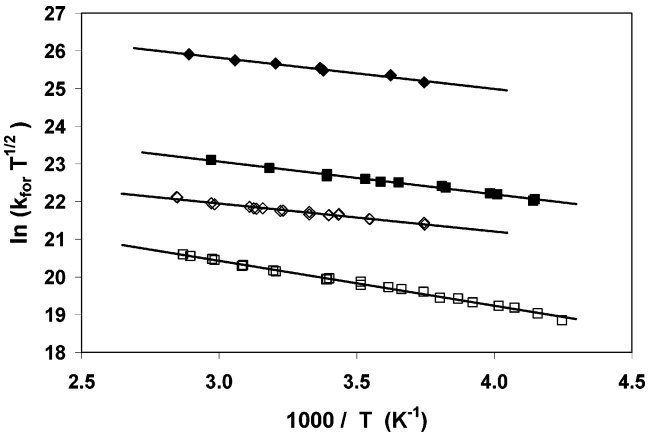

Figure 3. Plot of ln ($k_{for}T^{1/2}$) versus T^{-1} for C-shaped molecule **1** (filled symbols) and linear molecule **6** (open symbols) in benzonitrile (♦, ◊) and acetonitrile (■, □).

ground electronic state.[13] The free energy of the $S_1 \rightarrow$ CS reaction $\Delta_r G$ is given by

$$\Delta_r G = -RT \ln \frac{k_{for}}{k_{back}} \quad (8)$$

Figure 2 shows the dependence of the reaction free energy on the temperature for **1** in a set of substituted aromatic solvents, and Table 2 tabulates the experimental free energies in different solvents at 295 K. The experimental accessibility of the reaction free energy enables a critical (direct) test for models of solvation that are used in calculating the FCWDS term in eq 3 (vide infra). Unfortunately, reaction free energies more exoergic than −0.1 eV cannot be accurately determined by this method.

Within eq 3, the electronic coupling $|V|$ appears in the pre-exponent. Accordingly, $|V|$ can be determined from the temperature dependence of the electron-transfer rate constant. Figure 3 shows a plot of $\ln(k_{et}\sqrt{T})$ versus $1/T$ for **1** and **6** in two polar solvents. The slope of the temperature dependence is determined by the reaction free energy, the solvent reorganization energy λ_o, and $h\nu$, whereas the intercept (preexponential term) is determined by the electronic coupling $|V|$ and the Huang−Rhys factor S and depends weakly on λ_o. The Huang−Rhys factor S does not change significantly with solvents; thus, the shift in the rate constant intercepts for different solvents is largely a result of electronic coupling changes. The data in Figure 3 indicate that the electronic coupling for **1** in benzonitrile is significantly (3−4 times) larger than that in acetonitrile. In contrast, the coupling for the linear molecule **6** is the same in benzonitrile and acetonitrile. To quantitatively determine values of the electronic coupling $|V|$ and assess structure−reactivity correlations, the four parameters that determine the FCWDS in eq 3, $\Delta_r G$, λ_S, λ_V, and $h\nu$, need to be measured or adequately modeled.

Inner Sphere Reorganization. The internal reorganization energy λ_v and the effective mode frequency ν are commonly considered together and taken to be a characteristic feature of the solute, relatively independent of the solvent. For typical organic systems, like those shown in Scheme 1, one finds that characteristic vibrational frequencies in the range of 1400−1600 cm^{-1} constitute a dominant fraction of the reorganization energy changes in the high-frequency modes. In large part, this reflects the use of aromatic donor and acceptor moieties whose carbon−carbon bond lengths change considerably upon oxidation and reduction. Some workers have investigated the vibrational dynamics of molecules undergoing charge transfer through time-resolved vibrational spectra and/or resonance Raman spectroscopy;[8] however, most studies quantify the high-frequency mode parameters through kinetic studies, charge-transfer spectra, or quantum chemistry calculations. Our work has used the latter two approaches to quantify the reorganization parameters from quantum degrees of freedom.

For systems in which charge transfer spectra are detected, free energy and reorganization parameters can be extracted from the spectral position and line shape. Figure 4 illustrates this approach, which was quantitatively described by Marcus and others.[14] Panel A shows a free energy diagram to illustrate how the emission spectrum depends on the energy difference between the charge separated state and the ground electronic state, ΔG_{rec}, and the curvature of the surfaces. Using a single quantum mode expression for the charge transfer, the spectral shape is given by

$$I_{emission}(\nu') = F(n)\nu'^3_{fl} \sum_j \frac{e^{-S} S^j}{j!} \sqrt{\frac{4\pi^3}{h^2 \lambda_o kT}} |V|^2 \times \exp\left[-\frac{(jh\nu + \Delta G_{rec} + \lambda_o + h\nu'_{fl})^2}{4\lambda_o kT} \right] \quad (9)$$

where $F(n) = (16\pi^2 n/3)((n^2 + 2)/3)^2$. Although no charge-transfer emission bands were observed for donor−spacer−acceptor molecules **1**−**6** (Scheme 1), **7** exhibits strong charge transfer emission in nondipolar and weakly polar solvents. Internal reorganization parameters depend primarily on localized geometry changes in the electron donor and acceptor groups and should not be highly sensitive to their separation, so molecule **7** may be used to characterize λ_v and $h\nu$ for **1**. Panel B in Figure 4 shows a low-temperature spectrum in which vibronic structure is evident.[90] Panel C shows a room-temperature spectrum (note the residual asymmetry) for which spectral structure is no longer evident. Given the number of unknown parameters

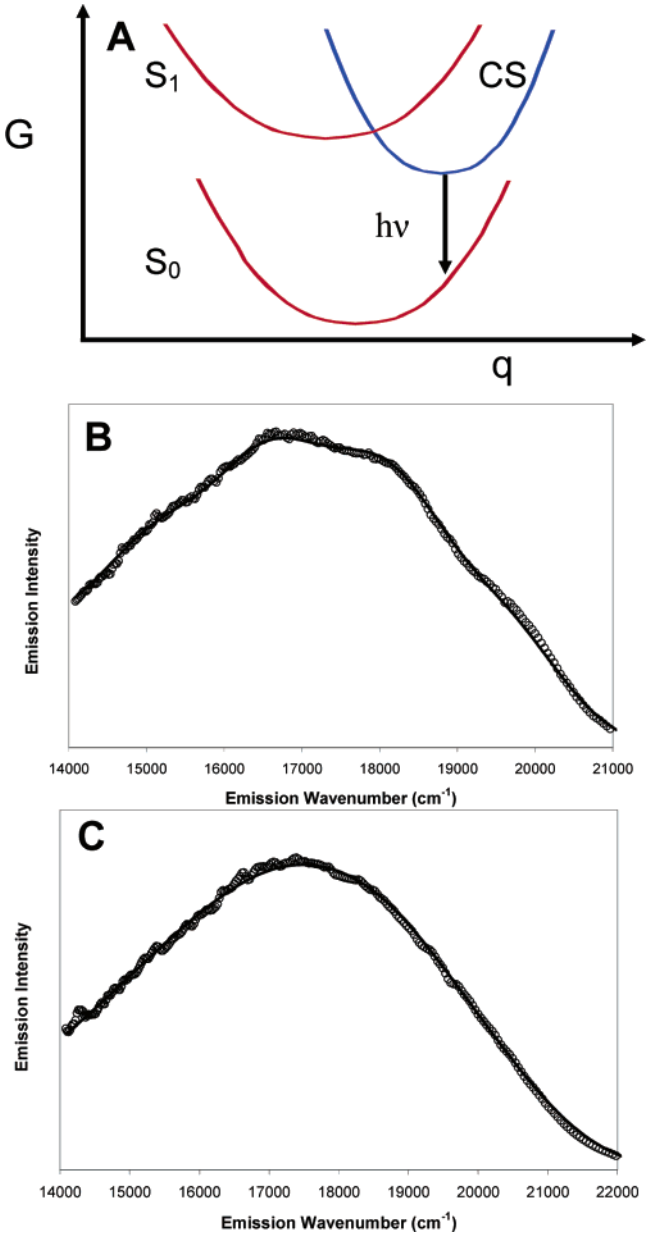

Figure 4. Panel A: potential surfaces responsible for the charge transfer (CT) emission spectrum. The CT emission spectra from molecule **7** at 170 K (panel B) displays a broadened vibronic progression that is not visible at 290 K (panel C). λ_V =0.393 eV and $h\nu$ = 0.186 eV are the best fit values used to fit the curves (solid lines) according to eq 9.

and the absence of structure in most charge-transfer spectra, accurate characterization of λ_v, $h\nu$, ΔG_{rec}, and λ_o, is possible only when charge-transfer absorption and charge-transfer emission spectra are both analyzed. The observation of vibrational structure in the low-temperature spectra of **1** makes the analysis sensitive to the values of λ_v and $h\nu$. Fitting of these and other spectra yields λ_v = 0.393 eV and $h\nu$ = 0.186 eV (Figure 4b). These results are similar to the best fit values determined from unstructured room temperature spectra in a series of weakly polar solvents, λ_v = 0.39 eV and $h\nu$ = 0.175 eV.[15] Hartree−Fock and MP2 calculations yield slightly larger values of λ_v.[16] The choice of λ_v and $h\nu$ affects the values of other kinetic model parameters (λ_o and $|V|$) that are obtained upon analysis of rate constant data. A detailed analysis of this dependence shows that relative electronic couplings for systems with the same donor and acceptor groups are slightly sensitive to changes in λ_v, (<15% for λ_v changes as large as 0.2 eV). Based on the room-temperature spectral analyses, the values of $h\nu$ and λ_v used for **1** are 0.175 and 0.39 eV, respectively.

Solvation

The remaining two parameters in the FCWDS, the reaction free energy and the outer sphere reorganization energy, are determined by solvation characteristics, i.e., solute−solvent interaction energies. The intrinsic reaction free energy depends on the difference in solvation energy for the neutral (reactant) species and the charge separated (product) species. The second moment of the solvation free energy is proportional to the solvent reorganization energy λ_o for the electron transfer. These quantities are often modeled by treating the solute as an electrostatic charge distribution within a cavity that is immersed in a dielectric continuum. With appropriate parametrization, such models can describe solvation energetics in polar solvents reasonably well,[17] and recent work by Kim[18] has extended these models toward nondipolar systems by incorporating quadrupole interactions. An alternative approach uses a molecular model that accounts for the discrete nature of solvent molecules and the solute by way of a pair distribution function. Our work uses a molecular model, developed by Matyushov,[19] to describe the solvation of **1**.[12,20−22] The experimentally determined reaction free energies for **1** in nondipolar and weakly polar solvents are used to parametrize the molecular model which can then be used to predict solvent reorganization energies and reaction free energies.

Continuum Models. The simple dielectric continuum models calculate solvation energies using a wavevector independent static dielectric constant ϵ_s and a high-frequency dielectric constant ϵ_∞.[17,23] The solute is treated as a spherical (or perhaps ellipsoidal) cavity containing a point source. In the case of bimolecular reactions, the model includes two spherical cavities, each containing a point charge, whereas for intramolecular electron-transfer reactions, it is more common to treat the solute as a cavity containing a dipole moment. The reaction free energy from this model is

$$\Delta_r G = \Delta_{vac} G - \frac{(m_{CS}^2 - m_{LE}^2)}{a_o^3}\left(\frac{\epsilon_s - 1}{2\epsilon_s + 1}\right) \qquad (10)$$

in which m_{LE} is the dipole moment of the initially excited state, m_{CS} is the dipole moment of the charge-separated state, and a_o is the cavity radius. The reaction free energy in a vacuum $\Delta_{vac}G$ provides a reference from which to include the solvation effect. The outer sphere reorganization energy λ_o may also be derived from the continuum model. For a dipolar solute in a spherical cavity, λ_o is given by

$$\lambda_o = \frac{(\Delta m)^2}{a_o^3}\left(\frac{\epsilon_s - 1}{2\epsilon_s + 1} - \frac{\epsilon_\infty - 1}{2\epsilon_\infty + 1}\right) \qquad (11)$$

where Δm is the magnitude of the dipole moment difference vector for the locally excited and the charge separated states, i.e., $\Delta m \equiv |\vec{m}_{CS} - \vec{m}_{LE}|$.

The solute molecule's characteristics are highly idealized in this continuum model. Its electrostatic potential is treated as a point dipole; its polarizability is ignored; and the details of its shape are lost. Using finite difference Poisson−Boltzmann (FDPB) methods, it is possible to extend continuum models to calculate both solvation and reorganization energies using a more realistic description of the solute molecule shape, ac-

TABLE 1: Solvent Parameters (Hard Sphere Diameter σ, Quadrupole Moment $\langle Q \rangle$, Dipole Moment μ, Polarizability α, Lennard-Jones Energy ϵ_{LJ}, Static Dielectric Constant ϵ_S, and High Frequency Dielectric Constant ϵ_∞)[a]

solvent	σ (Å)	$\langle Q \rangle$/D-Å	μ/D	α/Å^3 fitted	α/Å^3 lit.	ϵ_{LJ}/K	$(\langle Q \rangle/\lvert\mu\rvert\sigma)^2$	ϵ_s (295 K)	e_∞ (295 K)
benzene	5.3	8.2	0	11.2	10	602	∞	2.28	2.24
toluene	5.6	7.8	0.29	13.0	11.8	666	23	2.38	2.23
mesitylene	6.2	7.5	0	15.3	15.5	796	∞	2.27	2.24
TMB	6.2	7.3	0.30	16.0	15.5	778	15	2.38	2.26
cumene	6.25	7.8	0.24	16.7	16	760	26	2.38	2.22
1,3-DIP	6.7	7.8	0.21	19.7		920	30		2.21
TIP	7.4	8.1	0	27.2	31.8	1096	∞	2.25	2.21
DCT[b]	6.2	14.4 (5.6)	0.57	15.8	15.8	804	17 (2.5)		2.39
DCB	6.0	10.1	2.0		13.2	751	0.68	5.06	2.39
3-chlorotoluene	6.0	8.4	2.3		13.2	734	0.36	5.73	2.29
chlorobenzene	5.6	8.9	2.1		11.5	677	0.55	5.00	2.32
benzonitrile	5.7	15.3	4.8		12.5	432	0.31	25.9	2.33
acetonitrile	4.0	3.4	3.9		4	8	0.05	36.7	1.81
DMA	5.4	8.4	3.8		9.6	475	0.17	39.3	1.44

[a] TMB is 1,2,4-trimethylbenzene; 1,3-DIP is 1,3-diisopropylbenzene; TIP is 1,3,5-triisopropylbenzene; DMA is *N*,*N*-dimethylacetamide; DCT is 2,5-dichlorotoluene; DCB is 1,3-dichlorobenzene. [b] The value given for the quadrupole moment in parentheses represents that needed to obtain a good fit to the experimental free energy data. See text for details.

counting for its polarizability through an effective dielectric constant, and to incorporate a distributed charge distribution.[17] FDPB calculations were performed for **1** to determine whether its curvature and the presence of solvent within its cleft induced significant errors in simple continuum model predictions.[16] The simple and FDPB continuum methods produced similar estimates of $\Delta_r G$ for the highly polar solvent acetonitrile ($\epsilon_s = 37$), but the FDPB method predicted a smaller change in $\Delta_r G$, than predicted by the simple continuum model, upon changing to the less polar solvent THF ($\epsilon_s = 7.6$). Solvent entry into the cleft induced a small decrease of $\Delta_r G$ (-0.08 eV). The simple continuum treatments also use a highly idealized view of the solvent characteristics. More realistic treatments of the solvent response incorporate structural features on molecular and supramolecular length scales through the use of wavevector dependent dielectric constants. Such models have seen limited application in electron-transfer studies.[24]

Although they are easy to implement, continuum models have two significant drawbacks for these investigations. First, they are most reasonably applied to highly polar solvents, whereas many electron transfer processes in organic and biological systems occur in relatively nonpolar or weakly polar environments.[25] Second, continuum models yield erroneous predictions of the temperature dependence of the free energy and/or reorganization energy, even in polar solvents. This limitation was elucidated by Vath et al.,[26] who analyzed temperature-dependent charge-transfer spectra in different solvents and found that the reorganization energy decreases as the temperature increases, in contrast to the continuum model's predicted increase with increasing temperature in, e.g., acetonitrile

Molecular Model. Matyushov has developed a solvation model that accounts for the discrete nature of the solute and solvent and incorporates electrostatic, induction, and dispersion interactions between the molecules comprising the fluid.[19] This treatment computes reaction free energies and reorganization energies for charge-transfer reactions. This liquid-state model uses a reference fluid of hard spheres with diameter σ and treats the electrostatic interactions between the solute and solvent as perturbations. The solute is modeled as a sphere with a state-dependent, point dipole moment m_i and polarizability $\alpha_{0,i}$. The solvent is treated as a polarizable sphere, with an electrostatic charge distribution that is axial and includes both a point dipole and a point quadrupole. The relative importance of the solvent's dipolar and quadrupolar contributions to the solvation energy can be assessed through consideration of the ratio $(\langle Q \rangle^2/|\mu|^2\,\sigma^2)$. When this ratio is much larger than one, quadrupole interactions dominate; when it is one or smaller, dipole contributions dominate. The quantity $\langle Q \rangle$ is defined as $\langle Q \rangle = (^2/_3 \sum_i Q_{ii}^2)^{1/2}$ and represents the effective axial moment for the traceless quadrupole tensor.[27] Table 1 presents the value of this ratio for the solvents used to study the electron-transfer dynamics of **1**. It is evident from these simple considerations that quadrupole interactions should dominate in the weakly polar aromatic solvents and should be insignificant in highly polar and nonaromatic solvents.

In the molecular model, the reaction free energy $\Delta_r G$ is written as a sum of four terms

$$\Delta_r G = \Delta_{vac} G + \Delta_{dq,i} G^{(1)} + \Delta_{disp} G + \Delta_i G^{(2)} \qquad (12)$$

where $\Delta_{vac} G$ is the vacuum free energy, $\Delta_{dq,i} G^{(1)}$ contains first-order electrostatic and induction contributions, $\Delta_{disp} G$ contains dispersion terms, and $\Delta_i G^{(2)}$ contains second order induction terms. Correspondingly, the outer-sphere reorganization energy λ_o is written as a sum of three contributions

$$\lambda_o = \lambda_p + \lambda_{ind} + \lambda_{disp} \qquad (13)$$

where λ_p includes contributions arising from the solvent dipole and quadrupole moments, λ_{ind} includes contributions from induction forces, and λ_{disp} includes contributions from dispersion forces. Explicit expressions for the different terms in eqs 12 and 13 are presented elsewhere.[20] The experimentally determined reaction free energies for **1** as a function of temperature in non-dipolar and weakly dipolar solvents are used to calibrate the parameters in this model. After parametrization, the model is used to calculate the reorganization energy in the calibration solvents and to predict the reaction free energy and the reorganization energy in more polar solvents. A number of solvent parameters (in particular the solvent density ρ, polarizability α, effective hard sphere diameter σ, Lennard-Jones energy parameter ϵ_{LJ}, the dipole moment μ, and the quadrupole moment $\langle Q \rangle$) are required for this analysis, but they are available from the literature or can be calculated. For consistency, the dipole moment and quadrupole moments were computed for each solvent using quantum chemistry methods. The density, hard sphere diameter, and Lennard-Jones energy parameter were obtained from compiled tables,[28] based on fits to thermodynamic data of the solvents. The solvent polarizability was taken from literature data but was varied as much as 10% to obtain the

TABLE 2: Experimental Free Energies and the Predictions of Different Solvation Models for the Reaction Free Energy and the Solvent Reorganization Energy for Fourteen Different Solvents at 295 K[a]

solvent	Δ_rG, expt.	Δ_rG, $\langle Q\rangle$	Δ_rG, $(Q=0)$	Δ_rG, cont	λ_o, $\langle Q\rangle$	λ_o, $(Q=0)$	λ_o, cont
benzene	−0.111	−0.110	0.028	−0.043	0.178	0.027	0.008
toluene	−0.091	−0.083	0.024	−0.060	0.157	0.041	0.027
mesitylene	−0.043	−0.034	0.037	−0.042	0.111	0.033	0.006
TMB	−0.055	−0.052	0.020	−0.060	0.123	0.045	0.022
cumene	−0.054	−0.054	0.024	−0.061	0.123	0.038	0.031
1,3-DIP	−0.001	0.003	0.086		0.095	0.028	
TIP	0.001	0.007	0.043	−0.061	0.078	0.039	0.031
DCT	−0.103	−0.106	−0.049		0.147	0.084	
DCB		−0.474	−0.418	−0.290	0.545	0.484	0.247
3-chlorotoluene		−0.484	−0.451	−0.317	0.597	0.560	0.295
chlorobenzene		−0.458	−0.432	−0.288	0.558	0.530	0.258
benzonitrile		−0.762	−0.735	−0.485	0.902	0.872	0.470
acetonitrile	−0.55	−0.556	−0.553	−0.500	0.823	0.820	0.607
DMA		−0.677	−0.673	−0.502	0.792	0.789	0.733

[a] All values are given in eV. TMB is 1,2,4-trimethylbenzene; 1,3-DIP is 1,3-diisopropylbenzene; TIP is 1,3,5-triisopropylbenzene; DMA is *N*,*N*-dimethylacetamide; DCT is 2,5-dichlorotoluene; DCB is 1,3-dichlorobenzene.

best agreement between the measured free energies and the modeled values.

Previous parametrizations of this model for **1** were based on Δ_rG from homologous series of solvents.[20,21] For the purpose of this review, the molecular model was parameterized to provide accurate solvation data over as large a range of solvent polarity as possible. In addition, the electrostatic properties of **1** were modeled more accurately than previously by incorporating an S_1 state dipole moment of 7 D, which lies at 90° from the charge-transfer direction.[29] Figure 2 shows the experimental free energies Δ_rG for **1** in the alkylbenzenes, obtained directly from the kinetic data, and the reaction free energy in acetonitrile, determined by measuring the S_0 to S_1 transition energy, the oxidation potential of the donor moiety (1,4-dimethoxyanthracene), and the reduction potential of the acceptor moiety (dimethylmaleate). Good agreement between the experimental data and the model is obtained using solute parameters that are 0.38 eV for the vacuum free energy, $\Delta_{vac}G$, 7.48 Å for the cavity radius, and 14.6 Å^3 for the change in solute polarizability from S_1 to CS.[30] These parameters fail for one solvent, 2,5-dichlorotoluene; the experimental and calculated Δ_rG differ by 0.12 eV. The failure of the model may originate from the large and highly nonaxial quadrupole moment of 2,5-dichlorotoluene.[31] Table S1 in the Supporting Information summarizes the dipole and quadrupole tensor components for the different solvents. Although the effective quadrupole moment $\langle Q\rangle$ is used in the calculations, the nonaxial character of the charge distribution can still be significant. Gray and Gubbins[32] presented a formulation for solvation that accounts for the nonaxial contributions to the electrostatic energy. Its implementation for the system described here will require a major effort, and currently, there is insufficient data to confirm its validity. The nonaxial components to the electrostatic potential are most significant for 2,5-dichlorotoluene and benzonitrile, but solvation in the latter solvent is dominated by its dipole moment. An empirically based fit of the data that accounts for the nonaxial character provides reasonable fits to all of the data.[33] The alternative approach used here is to retain the simple axial model and adjust the quadrupole moment of 2,5-dichlorotoluene to an effective value. By reducing dichlorotoluene's quadrupole moment from 14.4 to 5.6 D Å^2 the experimental reaction free energy is well reproduced (Figure 2).

Although this parametrization generates reasonable fits to the experimental free energy data (alkylbenzenes, 2,5-dichlorotoluene, and acetonitrile), it is not possible to directly evaluate whether the parametrized model accurately reproduces quadrupole moment contributions to the solvation free energy and its temperature dependence in the polar solvents, for which experimental free energy data is not available. Based on the values of ($\langle Q\rangle^2/|\mu|^2\sigma^2$), solvation in the polar solvents should be dominated by the dipole terms (see Table 1). Table 2 presents the parametrized model's calculated reaction free energies in all of the solvents at 295 K for the appropriate value of $\langle Q\rangle$ and for the case of no quadrupole moment. Quadrupole contributions to the reaction free energy are significant for the alkylated benzenes, ranging from 0.07 to 0.1 eV. From comparison of the reaction free energies (at $Q=0$) in the cases of benzene, mesitylene, and TIP (recall $\Delta_{vac}G = 0.38$ eV), it is evident that the induction and dispersion terms contribute to Δ_rG in a significant way, ca. 0.3−0.4 eV. In 2,5-dichlorotoluene, the quadrupole moment makes a significant contribution to the reaction free energy; however, in the other chlorinated solvents, its influence is much less significant. For the case of 1,3-dichlorobenzene, the quadrupole accounts for about 6% of the total solvation free energy, as compared to about 30% in the alkylated benzene solvents. The contribution of the quadrupole moment to the total solvation energy becomes even less important as the dipolar character of the solvent molecule increases, in keeping with value of ($\langle Q\rangle^2/|\mu|^2\sigma^2$). Hence, the error in the solvation energy arising from the nonaxial nature of the quadrupole tensor probably does not significantly impact the calculated reaction free energies in the more polar solvents where experimental data is not available. Rather, its primary impact is in the nondipolar and weakly polar solvents where the experimental data can be used to calibrate its effect. This fortunate circumstance allows reliable and self-consistent modelling of λ_o and Δ_rG, thus enabling the extraction of electronic coupling magnitudes (vide infra).

The reorganization energies are calculated in a manner similar to the free energies. Table 2 presents λ_o predicted by the molecular model for the two different cases ($\langle Q\rangle$ and $Q=0$). Quadrupole contributions dominate the reorganization energy in the alkylbenzenes and 2,5-dichlorotoluene but play a minor role in the more polar solvents. A detailed presentation of the calculated reorganization energies and reaction free energies at 295 K are provided in the Supporting Information, Table S2. Induction terms also contribute to the reorganization energy but the dispersion contributions are minor. The reorganization energies predicted for the alkylbenzenes at 295K lie in the range of 0.08 to 0.18 eV. The reorganization energies in the more polar solvents are considerably larger than in the alkylbenzenes,

and are within 0.2 eV of the values derived from the FDPB continuum model.

Comparison and Assessment of the Solvation Models. Table 2 lists the available experimental $\Delta_r G$ data for **1** at 295 K and the values predicted by the parametrized molecular model and the simple continuum model. The best fit radius and $\Delta_{vac}G$ parameters from the molecular model also were used for the simple continuum calculations.[34] Both models predict similar qualitative changes upon increasing solvent polarity, but generate different detailed trends within similar solvents. Among the aromatic hydrocarbon solvents, the experimental $\Delta_r G$ becomes more positive as the alkyl content of the solvent increases. The continuum model does not reproduce this trend but the molecular model does, to within 9 meV. The molecular model succeeds in reproducing this trend because of the short-range nature of quadrupole solvation and the increasing hard-sphere solvent diameter upon increasing alkyl substitution of the aromatic ring. The inclusion of solvent quadrupolar interactions is required for accurate predictions of solvation in the aromatic hydrocarbon solvents (see Table 2), using a solute radius that also applies in polar solvents. An implementation of the molecular model[12] that excludes quadrupole interactions requires a significantly smaller solute radius to reproduce the experimental free energies in the alkylbenzenes. The smaller solute radius produces exceedingly large reorganization and reaction free energies in the more polar solvents.

The parametrized molecular and continuum models predict different $\Delta_r G$ values in the more polar solvents. Without experimental $\Delta_r G$ data in these solvents, it is not possible to determine the accuracy of either model. Experimental studies in the weakly polar solvent diethyl ether yield $\Delta_r G = -0.08$ eV for **1** at 295 K. The continuum model predicts $\Delta_r G = -0.21$ eV. The molecular model prediction, $\Delta_r G = -0.082$ eV, is much more accurate. Overall, the molecular model is quite good at reproducing room temperature $\Delta_r G$ values for which experimental data is available. The parametrized molecular model's predictions of the temperature dependence of $\Delta_r G$ come close, but do not exactly reproduce the available experimental data (Figure 2). Part of this failure may stem from the model's neglect of nonaxial terms in the quadrupole tensor.

The parametrized molecular and continuum models' predictions of the reorganization energy differ significantly. The continuum model predicts λ_o values in the alkylbenzene solvents that are more than 0.1 eV (more than 300%) smaller than the molecular model values (Table 2). The molecular model calculations with $Q = 0$ demonstrate that quadrupole interactions are the dominant source of solvent reorganization in the alkyl benzene solvents. The absence of quadrupole interactions within the continuum model is a primary reason for its small λ_o predictions in the alkylbenzene solvents. The continuum model predictions of λ_o in the polar, aromatic solvents are 0.3−0.4 eV smaller than the molecular model's predictions. Interestingly, the molecular and continuum model predictions of λ_o are in better agreement for the polar, nonaromatic solvents acetonitrile and dimethylacetamide. Continuum FDPB calculations[17] of λ_o for **1** in the latter two solvents[16] are even closer to the molecular model predictions listed in Table 2, but the FDPB prediction of λ_o for benzonitrile is again much smaller than the molecular model value. Calculations with $Q = 0$ (Table 2) indicate that solvent quadrupole−solute dipole interactions are not the source of the disparity in the λ_o predictions. Two points are clear: the continuum and molecular models generate very different $\Delta_r G$ and λ_o for solvents with significant quadrupole moments and consideration of the detailed molecular shape of **1** does

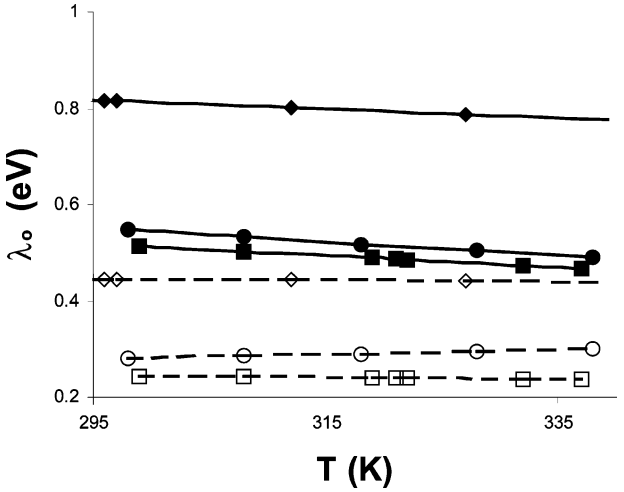

Figure 5. Predicted temperature-dependent reorganization energy for **1** in three solvents: benzonitrile (diamonds), chlorobenzene (squares), and meta-chlorotoluene (circles). The dashed lines and open symbols are for the continuum model, and the solid lines and filled symbols are for the molecular model.

significantly alter the continuum predictions. Without direct measurements of λ_o or $\Delta_r G$, it is not possible to determine whether either model accurately predicts solvation energies in polar aromatic solvents.

The molecular and continuum models also make different predictions for the temperature dependence of the reorganization energy. Figure 5 displays the two models' predictions for the reorganization energy as a function of temperature in three solvents. The molecular model (solid lines) predicts a negative slope for the reorganization energy in benzonitrile (◇), *meta*-chlorotoluene (○), chlorobenzene (□), and every other solvent in Table 2.[35] The continuum model predicts a positive slope of the reorganization versus temperature for **1** in *meta*-chlorotoluene, a slope of zero for benzonitrile, and a negative slope for chlorobenzene. Vath et al. have extensively studied the difference in the temperature dependences predicted by the two models.[26] The latter studies demonstrated that the molecular model correctly predicts a negative slope for λ_o versus temperature in cases where the continuum model failed, both quantitatively and qualitatively. The temperature dependence of the reorganization (and solvation) energy arises from two primary effects: density changes and increased thermal kinetic energy. The continuum model accounts indirectly for these effects, through the temperature dependence of the static dielectric constant, but does not include the effect of changing density in an explicit manner. The molecular model explicitly accounts for both of these effects on solvation energetics and, in addition, treats variations in the local solvent density.[26]

One can alter the continuum model predictions of λ_o and $\Delta_r G$ by varying the cavity radius and/or $\Delta_{vac}G$. For example, decreasing the continuum cavity radius and adjusting the vacuum free energy yields λ_o and $\Delta_r G$ values in the polar solvents that are closer to the molecular model predictions. However, this leads to unrealistic predictions for the nonpolar solvents. Furthermore, it does not correct the erroneous temperature dependence of λ_o in the polar solvents. Overall, the molecular model provides reasonable predictions of solvation related quantities for a wide of variety of solvents. The utility of the molecular model in these investigations arises, at least in part, from our ability to parametrize it with the experimental free energy data and from the relatively spherical shape of **1**. It may be that the model performs less well for solutes that deviate more strongly from spherical shapes. An advantage of con-

tinuum treatments is the ability to compute solvation energies for arbitrary solute shapes. The significantly different predictions, arising from the two solvation models, clearly illustrate the need for methods of measuring $\Delta_r G$ and λ_o in electron-transfer systems.

Obtaining the Electronic Coupling. Once internal reorganization energy parameters and reaction free energy data are available, one can extract values of the solvent reorganization energy and the electronic coupling by analyzing the temperature-dependent rate constant data. If the solvent reorganization energy and the electronic coupling were temperature independent, this process would be straightforward. However, the temperature dependence of the solvent reorganization energy and the possible temperature dependence of the electronic coupling parameter complicate such an analysis. In systems where the electronic coupling parameter is thought to be temperature independent, the rate constant data can be analyzed to extract a temperature-dependent reorganization energy $\lambda_o(T)$ and a value of $|V|$.[20,21] Such systems are likely to include donor−bridge−acceptor molecules in which the electronic coupling is mediated by a structurally rigid, intervening bridge (Scheme 1). By contrast, when the structures responsible for mediating coupling are assembled by noncovalent interactions and are highly mobile, both λ_o and $|V|$ may vary with temperature. The highly curved molecules studied here fall into this category. Fortunately, the molecular solvation model's accurate predictions of the temperature dependent reaction free energy data (see Figure 2) and the reaction free energy in acetonitrile at 295 K (see Table 2) suggest that the model, as parametrized, adequately mimics the solvation related properties of **1** for a variety of solvents and temperatures, with the notable exception of 2,5-dichlorotoluene. Taking the temperature dependent reorganization energy and reaction free energy from the model, the electronic coupling magnitude can be extracted directly from the rate data, via eq 3. This approach facilitates investigation of whether the electronic coupling has significant solvent and/or temperature dependence. The results of these investigations are summarized below.

Electronic Coupling

The electron transfer rate constant (eq 3) is proportional to the square of the electronic coupling, $|V|$, between the diabatic states at the curve crossing. In a one electron approximation, $|V|$ is the resonance integral for electron delocalization over the donor and acceptor. If no other atoms or molecules lie between the donor and acceptor, this coupling depends on the overlap of the donor and acceptor wave functions and exhibits a steep, exponential decrease with increasing separation. At separations greater than a couple of angstroms, simultaneous exchange interactions of the donor and acceptor with intervening molecules and atoms mediates the electronic coupling, generating larger interaction energies than does the direct interaction.[36]

Intervening molecules and ligands can mediate electronic interactions via a number of different mechanisms.[37,38] A superexchange model, elaborated by McConnell,[39] has received the most attention. Within this model, the initial and final diabatic states mix by virtue of their interactions with higher energy electronic configurations, e.g., obtained by promotion of an electron (hole) from the donor (acceptor) to an empty (filled) orbital of the intervening molecules. For the case of identical mediating sites and only nearest neighbor interactions, the electronic coupling V is given by

$$V = (T^2/\Delta)(-t/\Delta)^{N-1} \qquad (14)$$

where T is the interaction energy between the donor (acceptor) and the terminal superexchange orbital of the intervening structure, Δ is the energy difference between the diabatic transition state and the superexchange configurations involving the promoted electron (hole), and t is the interaction energy between the N adjacent bridge sites. This perturbation treatment is valid if t and T are much less than Δ. Two of the McConnell model's predictions for the dependence of the coupling on the structure of the intervening medium have sparked considerable investigation: (i) an exponential decrease of donor−acceptor coupling magnitude with increasing separation/number of sites (N) of the intervening medium, i.e., $\ln |V| \propto (N - 1)$, and (ii) the characteristic decay length for the interaction (i.e., the proportionality constant between $\ln |V|$ and N, commonly referred to as β), becomes small as (t/Δ) approaches one.[40]

Although the chemistry and physics is richer than shown by this simple model, detailed theoretical studies and experimental observations confirm these two essential aspects of the McConnell model.[41] Quantum calculations yield approximately exponential reductions of electronic coupling magnitudes with increasing separation in homologous spacer structures (linear alkanes, steroids, α-helix or β-sheet polypeptides, polyenes, stacked aromatics, etc).[40b,42] The net coupling magnitude is determined by a superposition of multiple coupling "pathways",[43] consisting of exchange interactions among adjacent sites and nonadjacent sites within the structure between the donor and the acceptor.[44] In addition, the majority of experimental studies report approximately exponential reduction of electronic coupling magnitudes with distance in a variety of media including organic glasses, DNA, proteins, organic, and inorganic spacers.[45,46] The predicted dependence of β on the energy gap[40,44c,47−49] has been probed, also. Paddon-Row et al.[40b] employed natural bond orbital (NBO) methods[50] to demonstrate that increasing Δ reduces the electronic coupling magnitude and increases the magnitude of β for π orbitals on opposite ends of an alkyl chain. Similarly, the coupling across B-form DNA exhibits an exponential decrease with distance, the steepness of which depends on Δ.[47,51] Recent theoretical efforts have explored the limits where t/Δ approaches one and the superexchange approximation breaks down.[37,52] These models involve excitation of the carrier (electron or hole) onto the bridging site(s) and "hopping" conduction through the spacer.

A number of studies report smaller β for electron-transfer reactions across aryl spacers (∼0.4) than for structurally similar spacers containing cycloalkane units.[5a,53] Spacer structural features that significantly lower mediating state energies appear to produce increased transfer rate constants.[5b,54,55] In an alternative approach, Miller varied Δ by altering the energy levels of the donors (by ∼2 eV), rather than the spacer and found that β for a low temperature glass varied systematically with the donor energy level.[56] As shown below, these two essential features of the McConnell description are also evident in solvent-mediated electron transfer.

Among the many electronic coupling investigations, few have identified contributions to the donor−acceptor coupling that are mediated by fluid solvent media. Electron transfer in organic glasses and transfer within and between proteins provide clear precedent that coupling does not require an entirely covalent pathway between the donor and the acceptor. However, the amplitudes of structural fluctuations in the fore-mentioned systems, although important,[57] should be much smaller than those of fluid solvents. Prior to the investigations summarized herein, a handful of experimental reports indicated that solvent molecules could mediate electronic coupling.[58−62] The direct

formation of solvent separated ion pairs from electronically excited acceptors in certain aromatic solvents provided a particularly convincing demonstration of solvent-mediated coupling.[63]

Our initial studies[15] indicated that detailed investigations of solvent-mediated coupling in unimolecular electron-transfer systems require donor−spacer−acceptor structural features that maximize solvent-mediated coupling and minimize through bond (through spacer) coupling contributions. At the minimum, (a) the spacer should juxtapose the donor and acceptor at a separation that is the smallest needed to accommodate an intervening solvent molecule in an appropriate orientation (vide infra), and (b) the spacer should include structural features that significantly reduce bond-mediated coupling magnitudes. Highly curved donor−spacer−acceptor molecules are one structural motif that meets these requirements. Alternatively, spacers might be able to promote solvent-mediated coupling through incorporation of molecular recognition elements that position a solvent or ligand directly between the donor and the acceptor.[64]

Although the experimental investigations of through-bond coupling and theoretical models provide general guidelines for understanding solvent-mediated coupling magnitudes, the involvement of solvent molecules in the coupling pathway introduces a number of unique structural issues. Solvent-mediated electronic coupling magnitudes should be dependent on the energies of solvent frontier molecular orbitals and on the distribution and nodal patterns of these orbitals, because they influence Δ, t, and T in eq 14. These issues are discussed in sections 1 and 2 below. Donor-to-acceptor separation can influence the sets of solvent configurations that provide effective coupling pathways. The contour of the solvent accessible cleft, defined by the spacer, donor, and acceptor groups, may also influence the accessible solvent configurations. These issues are discussed in section 3 below. Last, the motion of solvent molecules within the cleft causes the solvent-mediated coupling pathways and magnitudes to fluctuate. As the amplitudes of solvent motions are larger than the motions of "rigid" covalent spacers, solvent dynamics should modulate the magnitude of solvent-mediated coupling in C-shaped systems to a greater extent than normally occurs in linear donor−spacer−acceptor molecules. Solvent motion may lead to temperature-dependent electronic coupling magnitudes and/or a breakdown of the Condon approximation. These issues are discussed in section 4 below.

1. Solvent-Mediated Electronic Coupling: Theoretical Insights. In systems where t/Δ is much smaller than one, superexchange coupling magnitudes drop steeply with increasing number of superexchange sites, N, in a pathway (eq 14). For solvent-mediated coupling to approach the single site ($N = 1$) limit, the electron transfer active orbitals on the donor and the acceptor need to be sufficiently close to experience strong exchange interactions, T_{DS} and T_{SA}, *simultaneously* with the same orbital(s) of a single solvent molecule. For larger donor−acceptor separations (alternatively, for small solvents), a single solvent molecular orbital may not be large enough to interact with the donor and acceptor simultaneously. Because exchange interactions decrease very steeply with distance,[65] significant "through-space" jumps in coupling pathways will sharply diminish solvent-mediated coupling magnitudes.[66] Alternatively, solvent-mediated coupling pathways for larger donor-to-acceptor separations may include interactions among multiple solvent molecules ($N > 1$), but again, such couplings will be significantly smaller than for a single solvent molecule.

For a given solvent and donor−spacer−acceptor topology, the placement and orientation of a solvent molecule strongly

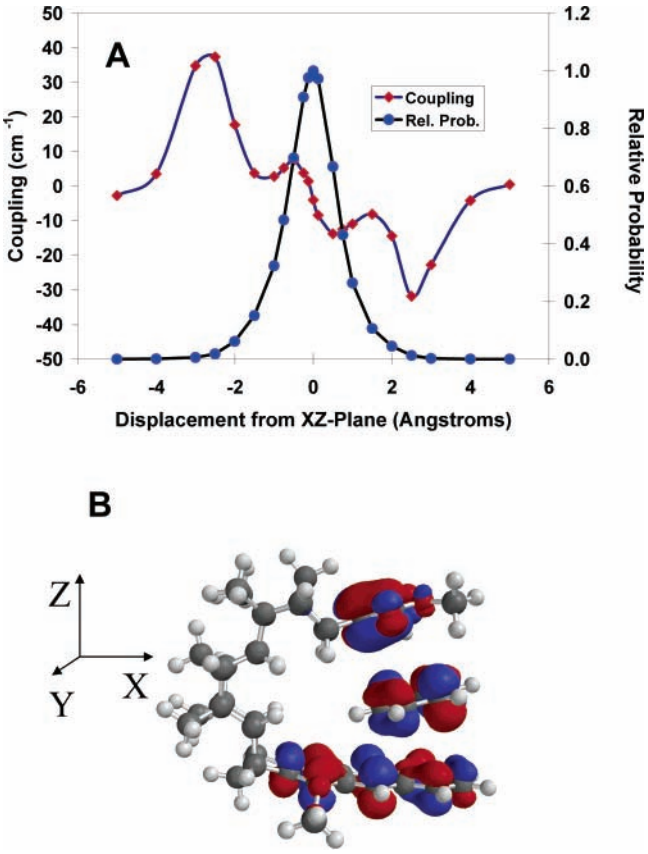

Figure 6. Panel A: Calculated values of the donor−acceptor electronic coupling (red diamond) for **1** as a function of the y displacement of a benzene solvent molecule. The positive y axis extends toward the viewer. The relative probability of each solvent configuration, as determined from molecular mechanics energies, is indicated by the blue filled circle. See the text for a more complete description. Panel B displays the reference frame, a ball-and-stick representation of the ground state, equilibrium geometry of **1** and the LUMO of the donor, benzene, and acceptor groups.

modulates the magnitude of solvent-mediated electronic coupling.[67] Donor-to-solvent and solvent-to-acceptor separations, relative orientations, and the nodal patterns of the electron-transfer active orbitals on the donor, acceptor, and solvent molecule all influence the magnitude of solvent-mediated coupling. Figures 6 and 7 present ZINDO−generalized Mulliken Hush (GMH)[68] calculated values of the donor−acceptor coupling for **1** as a function of a single benzene molecule's position and orientation within the cleft. For the purposes of this discussion, the reference frame is oriented with the x axis parallel to the long axis of the anthracene, the y axis parallel to the short axis of the anthracene, and the z axis perpendicular to the anthracene plane, roughly parallel to the direction of charge transfer. The origin lies at the center of the anthracene ring bearing the methoxy groups. Figure 6 displays the GMH coupling values for a benzene in a plane parallel to the anthracene group, displaced 3.6 Å along the z axis from the anthracene plane and oriented such that two benzene C−H bonds point in opposite directions along the x axis ("one H-up" configuration). The abscissa of this plot gives the distance, y, from the center of the benzene to the approximate symmetry (xz) plane of **1**. For benzene displacements larger than $y = \pm 5$ Å, $|V|$ is less than 5 cm^{-1}. Moving the benzene toward the xz plane increases the coupling magnitude until $y = \pm 2.5$ Å where $|V| = 35 \pm 3$ cm^{-1}. At this y value, the two benzene p orbitals closest to the xz plane are positioned to interact strongly with the p orbitals on the long edge of the anthracene and with two

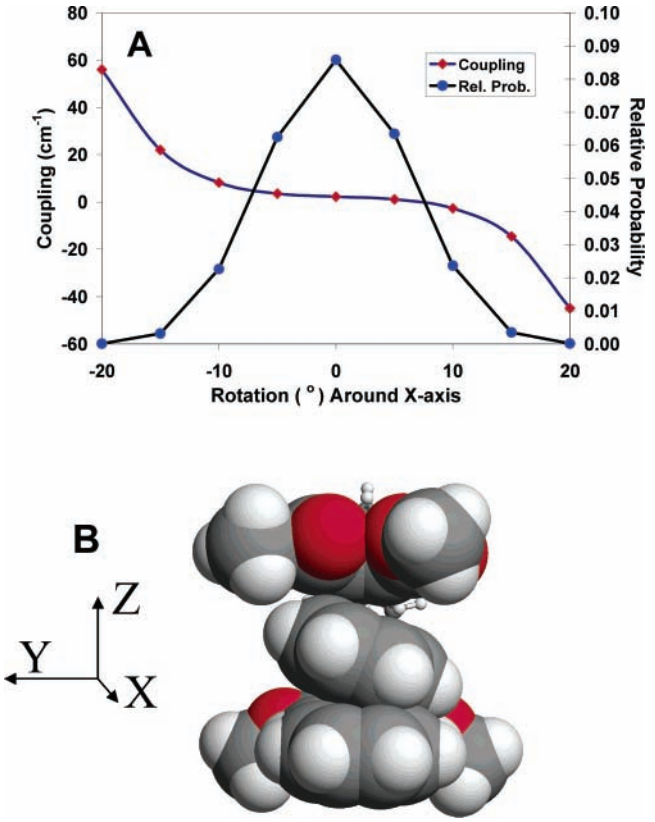

Figure 7. Panel A: calculated values of the donor−acceptor electronic coupling (red diamond) for **1** as a function of the rotation angle of a benzene about the *x* axis. The *x* axis extends toward the viewer. The relative probability of each solvent configuration, as determined from molecular mechanics energies, is indicated by the blue filled circle. For these calculations, the benzene was rotated by 30° about the *z* axis, relative to the benzene orientation in Figure 6. Panel B displays the reference frame, a ball and stick representation of the spacer, and CPK images of the donor, benzene, and acceptor groups, with the benzene oriented at −20° about the *x* axis.

adjacent, in phase carbons (bold) of the O=**C**−**C**=C portion of the acceptor LUMO. Further movement of the benzene toward the *xz* plane reduces $|V|$ to ∼0 cm^{-1} at $y \sim 0$ Å. The solvent-mediated coupling is insignificant at geometries near $y = 0$ because the electron-transfer active LUMOs of the donor and acceptor have different symmetry with respect to the *xz* symmetry plane (a′ and a″ respectively) and the orbitals of the solvent also transform as a′ and a″ when near the symmetry plane, making for a small mixing. The change of sign in the profile of *V* versus *y* reflects the nodal properties of the donor and acceptor. When the benzene is positioned close to the *xz* plane, solvent-mediated interactions on the $y > 0$ and $y < 0$ sides are of similar magnitude but opposite signs, resulting in near cancellation of the coupling. Although the absolute sign of the electronic coupling has no impact on an electron transfer rate constant, the relative signs of two contributing interactions does influence the coupling magnitude and the transfer rate constant. A qualitatively similar, but quantitatively different, behavior is also seen for other orientations of the benzene molecule and displacement along other directions, e.g., *x* displacement. (See Chart 2 in the Supporting Information.) Solvent molecule rotations also cause strong variation of coupling magnitude. Figure 7 displays the coupling predicted for a benzene molecule, positioned on the *xz* symmetry plane ($y = 0$), as a function of the rotation angle about the *x* axis. Positive rotations position the left half of the benzene closer to the left half of the donor and position the right half of the benzene closer to the right half of the acceptor. For rotation angles $|\phi_x| < 10°$, the coupling magnitude is close to 0 cm^{-1}, but for $|\phi_x| \geq 10°$, the coupling magnitude rises steeply, achieving values close to 60 cm^{-1} at 20°. These rotations replace the destructive interference present at small angles with a single set of strong interactions at larger angles. Rotations of the benzene about the *y* axis induce similar variations of the coupling magnitude. (See Chart 3 of the Supporting Information.)

The above results reveal a complex dependence of solvent-mediated coupling sign and magnitude on the location and orientation of a solvent molecule in the cleft. This strong dependence of coupling on nuclear geometry, for a readily accessible portion of solvent configuration space, constitutes a significant difference between solvent-mediated coupling and bridge-mediated coupling. It creates the possibility for unique properties/behavior of solvent-mediated coupling and also alters the interpretation of "measured" coupling values. In the non-adiabatic limit, the probability of electron transfer during any single reactant/product crossing event *j* is proportional to the square of the particular value of the coupling, $(V_j)^2$, where V_j depends on the current "in-cleft" solvent configuration. During subsequent crossing events, the instantaneous values of the electronic coupling will be different because of variation in the in-cleft solvent configuration. Assuming that the probability and energy of any particular in-cleft solvent configuration, E_j, is independent of the "bulk" solvent configurations required to access the level crossing (transition state), the experimentally observed electronic coupling can be expressed as an ensemble average of the values at the configurations *j*, namely

$$\langle |V|^2 \rangle = \frac{\sum_j |V_j|^2 \exp(-E_j/kT)}{\sum_j \exp(-E_j/kT)} \qquad (15)$$

Figures 6−7 display plots of the Boltzmann factors (relative probabilities) for the solvent configurations whose couplings were calculated. Because the fluctuations of solvent-mediated coupling magnitude are large[69] among the accessible solvent configuration, environmental variables such as temperature or pressure, which alter the relative populations of the solvent configurations, may alter the observed magnitude of solvent-mediated coupling. Evidence for these effects will be discussed below.

2. Energy Gap Effects on Coupling. The electronic coupling depends on both the site-to-site exchange interactions and on the energy gap, Δ, between the electron-transfer transition state and the superexchange state. The energy gap for electron-mediated superexchange involving a single solvent may be estimated as[70]

$$\Delta \sim \mathrm{IP(D^*,vertical)} - \mathrm{EA(S,vertical)} + C_{MS}(\mathrm{D+,S-}) + \Delta G_{TS\_SOLV} \qquad (16)$$

where IP(D*,vertical) is the vacuum, vertical ionization potential of the excited donor, EA(S,vertical) is the vacuum, vertical electron affinity of the solvent, C_{MS}(D+,S−) is the vacuum Coulomb interaction between the charged donor and solvent in the transition state geometry, and ΔG_{TS_SOLV} is the differential solvation energy, arising from the solvent polarization at the transition state interacting with the superexchange state dipole moment minus its interaction with the D*SA state dipole

TABLE 3: Solvent-Mediated Electronic Coupling Magnitude and Distance Dependence

solvent	LUMO (eV) 6-31G**	EA (eV) expt.	IP (eV) expt.	$\|V\|$ (cm^{-1}) for **1**	$\|V\|$ (cm^{-1}) for **3**	β (1/Å)
benzonitrile	2.44	0.24	9.7	12	2.8	0.97
1,3-dichlorobenzene	3.14	−0.31	9.1	7.7		
2,5-dichlorotoluene	3.18	−0.31	8.8	6.1		
o-dichlorobenzene	3.20	0.094	9.2	9.0	2.8	0.78
CH_2Br_2	3.20		10.2		2.8	
$CHCl_3$	3.29		11.4		2.5	
$(C_6H_5)CH_2CN$	3.43		9.4		2.2	
CH_2ClBr	3.55		10.8		2.4	
chlorobenzene	3.57	−0.75	9.1	8.5		
3-chlorotoluene	3.60	−0.75	8.7	7.5		
anisole	3.93		8.4		1.6	
veratrole	4.01		7.8		1.3	
cumene	4.04		8.7	5.2		
benzene	4.05	−1.12	9.2	7.2		
toluene	4.06	−1.11	8.8	6.9		
1,3-dithiolane	4.08		8.8		1.9	
mesitylene	4.17	−1.03	8.4	4.9		
CH_2Cl_2	4.19		11.3	5.2	2.0	0.64
1,2,4-trimethylbenzene	4.20	−1.07	8.4−8.6	5.6		
1,3-diisopropylbenzene	4.3			4.4		
1,3,5-triisopropylbenzene	4.4		8.2	3		
tetrahydrothiophene	5.30		8.4		1.4	
N,*N*-dimethylacetamide	5.56		9.2	6.3		
acetonitrile	5.77		12.0	4.6	1.1	0.95
tetrahydrofuran	6.21		9.4		1.1	
diethyl ether	6.46		9.5	3.5	0.9	0.91

moment. $|\Delta G_{TS\_SOLV}|$ contributes less than −0.3 eV.[70] The second term on the right-hand-side of eq 16 introduces particular sensitivity to the nature of the solvent.[71] Solvents with more positive electron affinity yield smaller Δ and, therefore, should provide larger coupling. This prediction was tested for molecules **1** and **3**. Table 3 lists values of $|V|$ for **1** in various solvents at 295 K, obtained using the molecular solvation model to calculate the FCWDS (vide supra). The largest coupling, in benzonitrile, is four times larger than the smallest coupling, in 1,3,5-triisopropylbenzene. GMH calculations for **1** in the absence of solvents indicate negligible bond-mediated coupling (<0.5 cm^{-1}).[67b,72] Values of EA(S,vertical) for the solvents in Table 3 are needed to employ eq 16 but have not been reported for all of the solvents. Instead, EA(S,vertical) has been calculated as the 6-31G** LUMO energy at each solvent's ground-state equilibrium geometry and scaled to the known experimental EA(S,vertical) values.[73]

For **1**, the cleft defined by the donor, spacer, and acceptor is large enough to accommodate at most one solvent molecule. Thus, the $N = 1$ limit of eq 14 applies and $|V| = T_{D^*S}T_{SA}/\Delta$. Substituting eq 16 into this expression and rearranging yields

$$\frac{1}{|V|} = -\frac{\mathrm{EA(S,\,vertical)}}{T_{D^*S}\,T_{SA}} + \frac{\mathrm{IP(D^*,\,vertical)} + C_{MS}(\mathrm{D+,S-}) + \Delta G_{TS\_SOLV}}{T_{D^*S}\,T_{SA}} \quad (17)$$

A plot of $|V|^{-1}$ versus −EA(S,vertical) (Figure 8A) shows a discernible trend of increasing $|V|^{-1}$ for solvents with more negative vertical electron affinity, albeit with scatter. The size and number of substituents on the periphery of the aromatic solvents influence the coupling magnitude, presumably because of steric constraints on the set of available solvent-in-cleft configurations (vide infra). The figure divides the solvents for **1** into two classes, bulky (unfilled triangles) and not bulky (shaded triangles). Ignoring the bulky solvents yields a plot with a clearer correlation between $|V|^{-1}$ and the solvent molecule's vertical electron affinity. This correlation supports the predominant role of solvent in mediating electronic coupling in **1**. Figure 8B shows a similar analysis but uses the solvent's ionization potential for which a correlation is expected if hole-mediated superexchange pathways are important. In this case, no correlation is evident. These observations show that coupling pathways with electron excitations to the bridge, rather than hole excitations, dominate the interaction.

An estimate of the configurational average of $(T_{D^*S}T_{SA})$ can be obtained from a linear regression analysis of Figure 8A according to eq 17. Excluding values for the trisubstituted aromatic solvents, the slope of the regression line for **1** is 270 eV^{-2}. This slope provides a geometric mean $[(T_{D^*S}\,T_{SA})^{1/2}]$ for the two exchange terms of 490 cm^{-1}. Excited donor−solvent and solvent−acceptor diabatic state interaction energies are determined as part of the GMH analyses (see Figures 6 and 7). The root-mean-square interaction energy averaged over the solvent configurations amounts to 400 cm^{-1}. The correspondence between these two estimates is much better than one should expect given the approximate nature of the determinations.

In the C-shaped molecule **3**, the distance between the anthracene donor and the nitroethylene acceptor is 10 Å, about 3 Å larger than in **1**. The increased width of the cleft enables entry of larger solvent molecules and affords in-cleft solvent molecules greater freedom of placement and orientation as compared to the cleft of **1**. Molecular mechanics studies indicate that the cleft is still too small to accommodate more than one solvent molecule. The absence of detectable equilibrium between the charge-separated and locally excited states in this molecule precludes parametrization of the molecular solvation model. Instead, the FCWDS for **3** in each solvent is estimated from the experimental rate constant of the linear molecule, **9**, that contain the same donor and acceptor and approximately the same center-to-center charge-transfer distance.[74] Table 3 lists the resulting values of $|V|$ for the excited-state charge separation reaction of **3** in the investigated solvents. The couplings for **3**, which range from 1 cm^{-1} in diethyl ether to 3 cm^{-1} (methylene dibromide, benzonitrile, and *o*-dichlorobenzene), are considerably smaller than for **1**, because **3** has a larger cleft and hence larger donor-to-solvent and solvent-to-acceptor distances. GMH

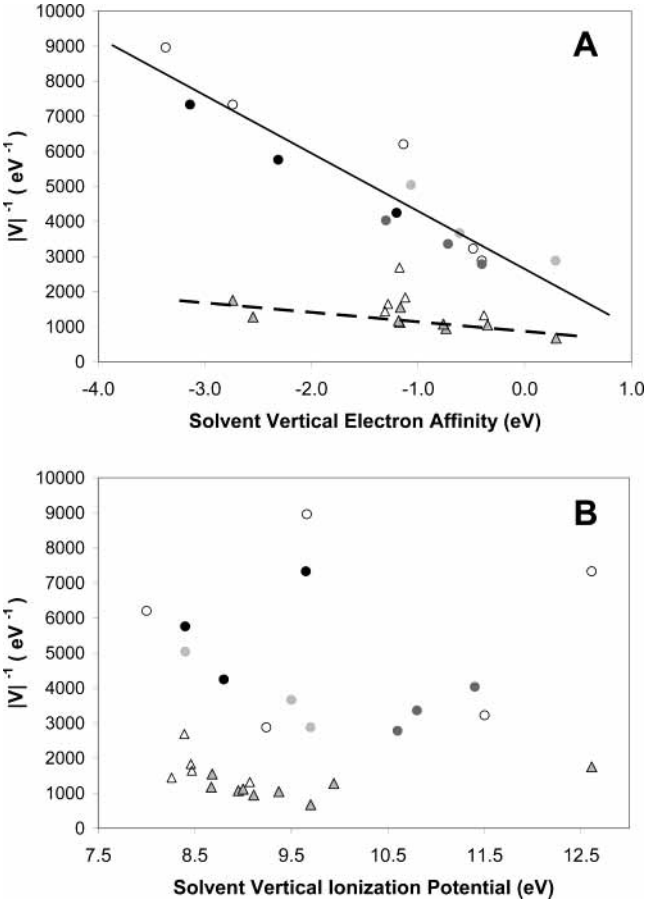

Figure 8. Panel A: Reciprocal of the electronic coupling magnitude plotted versus the vertical electron affinity for each solvent. The regression line for **1** (— —) was calculated using data from all solvents (▲) with the exception of the trisubstituted aromatic solvents (△). The regression line for **3** (solid line) was calculated using data from all the solvents (circles). The data from **3** in five member ring, nonaromatic solvents (●), CH_2X_2 solvents (shaded circles), and monosubstituted aromatic solvents (light shaded circles) are indicated to demonstrate the reduction in scatter among structurally similar solvents. Panel B: The reciprocal of the electronic coupling magnitude is plotted versus the vertical ionization potential of each solvent for **1** and **3**. The shadings indicate the same solvents as in panel A.

calculations for **3** predict spacer-mediated coupling of <1 cm^{-1}. Thus, a portion of the experimentally determined couplings may arise via the spacer. With that caveat, $|V|^{-1}$ for **3** exhibits a marked dependence on the solvent vertical electron affinity, EA(S,vertical) (Figure 8A).

If an aromatic solvent within the cleft of **3** is oriented with its molecular plane parallel to the donor and acceptor groups (as is sterically enforced in **1**), the donor−spacer and spacer−acceptor separations would be, on average, 1.5 Å greater for **3** than for **1**. Accordingly, $(T_{D^*S}\ T_{SA})^{1/2}$ for **3** would be 40 times smaller than for **1**.[75] A linear regression analysis of the data for **3** in Figure 8a yields 200 cm^{-1} for $(T_{D^*S}\ T_{SA})^{1/2}$ which is only two and half times smaller than the value for **1**. This result suggests that a solvent molecule within the cleft orients to maximize van der Waals contact with the donor and the acceptor. Such rotated solvent configurations reduce the length of through space gaps in the tunneling pathway for the wider cleft and may account for the small decrease in $(T_{D^*S}\ T_{SA})^{1/2}$.[76]

3. Structural Factors of the Solvent and Donor−Spacer−Acceptor Molecules. The observation that $(T_{D^*S}\ T_{SA})^{1/2}$ for **1** is two times larger than for **3** demonstrates that cleft width influences the magnitude of T_{D^*S} and T_{SA} exchange interactions. Most likely, cleft width, solvent size, and the mediating orbital distribution collectively influence $(T_{D^*S}\ T_{SA})^{1/2}$. The variety of effects that solvent structure can induce is revealed by consideration of the data in Table 3 and the scatter in the plots of $|V|^{-1}$ versus electron affinity (Figure 8A). As noted previously for **1**, the couplings determined in aromatic solvents with sterically demanding substituents are significantly smaller than the couplings determined for less sterically demanding solvents with similar electron affinity. Thus, although benzene and toluene provide a coupling of $\sim$7.1 cm^{-1}, the presence of three peripheral alkyl carbons in 1,3,5-trimethylbenzene (mesitylene), 1,2,4-trimethylbenzene, and isopropylbenzene (cumene) provide a 27% smaller $|V| \sim 5.2$ cm^{-1}. The presence of a second isopropyl group in 1,3-diisopropylbenzene reduces the coupling further (to 4.5 cm^{-1}) relative to cumene, and a third isopropyl group on the aromatic ring periphery (1,3,5-triisopropylbenzene) yields the smallest coupling of all of the solvents investigated with **1** (3 cm^{-1}). As the vertical electron affinities of all of these solvents are similar, the decrease of $|V|$ with increasing numbers of alkyl groups originates from a decrease of the average value of $(T_{D^*S}\ T_{SA})^{1/2}$.

The values determined for $|V|$ and for $(T_{D^*S}\ T_{SA})^{1/2}$ reflect an average over all solvent−cleft configurations (including vacant clefts) that are present at the electron-transfer transition state. Increased steric repulsion, between the alkyl groups along the periphery of the solvent and the donor−spacer−acceptor contour defining the cleft, reduces the net coupling (i) by favoring in-cleft solvent configurations that have small solvent π-system overlap with one (or both) of the donor and acceptor groups or (ii) by favoring vacant-cleft solvent configurations. The lowest energy conformation of an aryl bonded isopropyl group projects its methyl groups above and below the aromatic plane. The presence of three of these alkyl "bumpers" around the aromatic periphery in triisopropylbenzene greatly reduces the fraction of solvent configurations for which the solvent molecule's π system lies within the cleft and reduces the exchange interaction for those configurations in which the π system makes it into the cleft. Given the steric barrier, it is possible that the $|V|$ of 3 cm^{-1} determined for triisopropylbenzene reflects tunneling that is mediated primarily by the isopropyl groups. The coupling in this system is small because the solvent is too big to "fit" within the cleft. The size and distributions of alkyl groups in the other alkylbenzene solvents do not prevent solvent entry into the cleft; however, they provide less coupling than observed for benzene as a result of the two effects noted above (vide infra − dynamics).

In contrast to **1**, the larger cleft of **3** readily accommodates a single solvent molecule for each of the solvents in Table 3. Rather, the "challenge" for solvents is to span the increased donor acceptor separation within **3** without using more than one solvent molecule ($N > 1$ limit). For a good "fit" with **3**, a solvent must provide a LUMO of wider extent than for **1**. Consequently, one might expect the mean values of $(T_{D^*S}\ T_{SA})^{1/2}$ to vary with solvents to a greater extent than with **1**. The effect of solvent size and shape on $(T_{D^*S}\ T_{SA})^{1/2}$ can be examined by dividing the data into three solvent categories: nonaromatic five-member ring, monosubstituted aromatic, and CH_2X_2. Within each solvent set, a reasonably linear correlation is observed (Figure 8A). The slopes of the regression lines through all three subsets are similar, yielding $(T_{D^*S}\ T_{SA})^{1/2}$ of 200, 210, and 220 cm^{-1}, respectively. Surprisingly, despite their different sizes and shapes, all three sets of solvents generate comparable values of $(T_{D^*S}\ T_{SA})^{1/2}$.

The distance dependence of solvent-mediated coupling can be probed using **1** and **3**, which both can accommodate only one solvent molecule in its cleft. For the solvents in which both molecules were studied (see Table 3), the electronic coupling for **1** (7.1 Å gap) is three to four times larger than for **3** (9.9 Å gap). This reduction in coupling corresponds to an effective tunneling decay constant β ranging from 0.64 to 0.97 per Å for the five solvents (see Table 3). Paddon-Row and co-workers studied electron transfer in two highly curved U-shaped molecules whose spacers provided 7.5 and 9.5 Å separations between identical donor and acceptor pairs.[66] The reduction of optimal electron-transfer rate constants with increased donor/acceptor separation in their system yields β values between 0.3 and 1 $Å^{-1}$.[77] For the polar solvents investigated using both the U-shaped and C-shaped molecules, *o*-dichlorobenzene and acetonitrile, similar β values are obtained. As the clefts of all four molecules are too narrow to accommodate two solvent molecules, the β values reflect changes in the ensemble average of $(T_{D*S}\ T_{SA})^{1/2}$ with increasing separation, rather than an increase in the number of superexchange sites. Paddon-Row et al. proposed that the distance dependence of solvent-mediated coupling might be nonmonotonic.[66] In their model, $|V|$ would decrease sharply for cleft widths larger than an integral number of solvent diameters because of inefficient tunneling ($\beta = 2.8$ $Å^{-1}$) across the gaps between the solvents. However, $|V|$ would increase sharply at cleft widths corresponding to the next integral number of solvents, generating a zigzag coupling versus distance profile. For the nonspherical solvents employed in both of our investigations, the distance dependence of $|V|$ is shallower than predicted and likely results from the ensemble of single solvent orientations and placement available at the investigated cleft widths. Cleft shape, solvent size and shape, and the ensemble of solvent configurations clearly play important roles in determining the distance dependence of solvent-mediated coupling.[78]

4. Dynamical Effects on Solvent-Mediated Coupling Magnitudes. Motions of solvent molecules comprising the electron tunneling pathway modulate the magnitude and sign of the electronic coupling matrix element. The GMH studies allow calculation of a Boltzmann weighted, ensemble average value of $|V|$ according to eq 15.[79] For the 78 configurations of a single benzene in the cleft of **1**, the ensemble average value of the root-mean-square coupling is $\langle V^2\rangle^{1/2} = 14.8\ cm^{-1}$ at 298 K. The ensemble average of the coupling is $\langle V\rangle = -0.6\ cm^{-1}$ and the root-mean-square deviation from the average is $\delta \approx \langle (V - \langle V\rangle)^2\rangle^{1/2} = 14.8\ cm^{-1}$. The coupling fluctuations are large relative to the mean coupling value.[80] This feature distinguishes solvent-mediated coupling from bridge-mediated donor−acceptor coupling, for which the structure, not structural fluctuations, is the primary factor determining through-bond coupling magnitudes.[15,69b,c] If the experimental values of solvent-mediated coupling magnitude reflect an ensemble average (eq 15), external factors that change the energies or relative probabilities of the individual solvent configurations should alter the observed coupling magnitude. For example, changing the temperature to 400 K for the ensemble of 78 benzene/**1** solvent configurations increases the root-mean-square coupling, $\langle |V|^2\rangle^{1/2}$, to 16.5 cm^{-1}. The larger coupling arises from increased population of higher energy, larger coupling solvent configurations. This percentage change in $\langle |V|^2\rangle^{1/2}$ would increase *both* k_{for} and k_{back} by 20%.

The electron-transfer rate constants for **1** exhibit a variety of temperature dependences. In solvents containing polar groups (C−Cl, −CN, and −C(O)NMe_2), k_{for} ($S_1 \rightarrow CS$) increases with increasing temperature. These solvents are too polar ($\Delta_r G$ is more negative than −0.15 eV) to generate significant values of

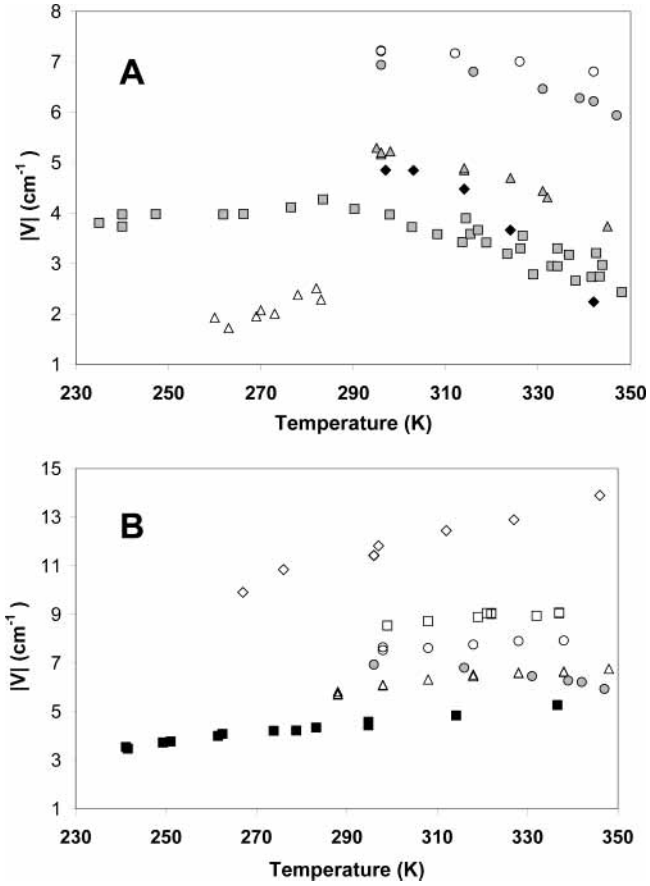

Figure 9. Panel A: Temperature dependence of the donor−acceptor electronic coupling for **1** in nondipolar aromatic solvents: benzene (○); toluene (shaded circle); cumene (shaded triangle); mesitylene (♦), 1,3-diisopropylbenzene (shaded square); 1,3,5-triisopropylbenzene (△). Panel B: The temperature dependence of the donor−acceptor electronic coupling for **1** in polar aromatic solvents and toluene: benzonitrile (◊), chlorobenzene (□), *meta*-chlorotoluene (○), toluene (shaded circle), 2.5-dichlorotoluene (△), acetonitrile (■).

k_{back} ($CS \rightarrow S_1$), with the exception of 2,5-dichlorotoluene. In benzene and the monosubstituted alkyl aromatic solvents, toluene and cumene, k_{for} decreases and k_{back} increases with increasing temperature.[12] The opposite temperature slopes of k_{for} and k_{back} originate from a change in the sign of $\Delta_r G$ (from negative to positive) upon increasing the temperature. The temperature dependence of the rates in the multiply alkylated aromatic solvents vary widely. In 1,2,4-trimethylbenzene, the rate constants exhibit trends similar to benzene; k_{for} decreases and k_{back} increases with increasing temperature. In the bulkier solvent 1,3,5-triisopropylbenzene, k_{for} and k_{back} both increase with increasing temperature (260 to 290 K). For 1,3-diisopropylbenzene and mesitylene, the rate constants vary nonmonotonically with temperature. In 1,3-diisopropylbenzene, k_{for} increases from 220 to 270 K and decreases from 290 to 360 K, whereas k_{back} increases from 220 to 300 K and decreases above 330 K.[81] In all solvents, the rate versus temperature profiles are heavily influenced by the temperature dependence of the FCWDS. Any temperature dependence of $|V|$ can be examined only after the FCWDS has been quantified. Fortunately, the molecular solvation model has been calibrated for **1** (vide supra) and provides a means to calculate $\lambda_o(T)$ and the FCWDS(T) and to extract values of the coupling as a function of temperature directly from the experimental electron-transfer rate constants (see Figure 9).

The solvation model does a fair job of reproducing the experimental $\Delta_r G(T)$ data for the charge separation reaction of

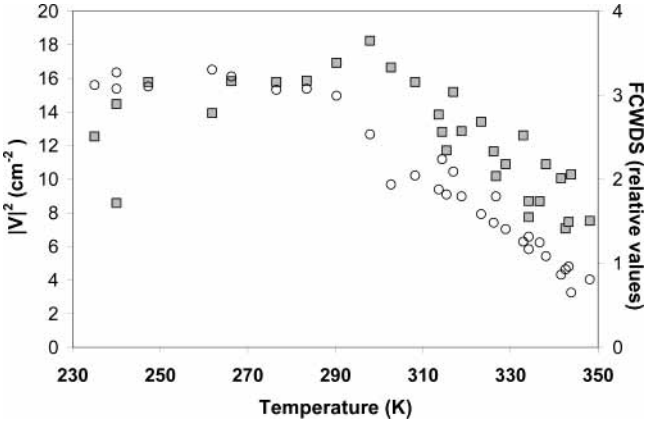

Figure 10. Contributions of $|V|^2$ (shaded square, left *y* axis) and the FCWDS (○, right *y* axis) to the temperature dependence of the charge separation rate constant for **1** in 1,3-diisopropylbenzene. The FCWDS were calculated using the experimental values of $\Delta_r G$ and the parametrized solvation model values of the λ_o.

1 in the hydrocarbon aromatics. As such, the model's estimates of $\lambda_o(T)$, the resulting values of the FCWDS, and the extracted $|V|$ in these solvents should be reasonably accurate. For **1** with the hydrocarbon aromatic solvents, $|V|$ appears to decrease with increasing temperature, with the sole exception of triisopropylbenzene (TIP, see Figure 9). For benzene, the coupling change is very small, amounting to a 5% reduction over a 50 K range. The coupling decrease in toluene is twice as large, $\sim -10\%$ over a 50 K range. The solvation model reproduces $\Delta_r G$ very accurately for these two solvents. Thus, the predicted λ_o and the estimated FCWDS are as accurate as can be achieved currently. Interestingly, these results differ from the prediction based on the ensemble average of GMH calculated couplings for "in-cleft" configurations (vide supra). The solvation model accurately predicts $\Delta_r G$ for cumene between 295 and 332 K ($|\delta\Delta_r G| \equiv |\Delta_r G(\text{expt.}) - \Delta_r G(\text{model})| < 5$ meV)). Over this temperature range, the calculated FCWDS decreases by less than 30%, however k_{for} decreases by nearly 60%. This indicates that $\langle|V|^2\rangle$ decreases by more than 30%. This is credible evidence that $|V|$ decreases with increasing temperature for **1** in cumene.

Similar conclusions are obtained by analyzing the rate, FCWDS, and $|V|$ results for **1** in mesitylene. The solvation model somewhat underestimates the (positive) slope of $\Delta_r G(T)$ in mesitylene, yielding values of $\delta\Delta_r G$ equal to -7 meV at 297 K and $+6$ meV at 347 K (<20% error). Nonetheless, using the shallower $\Delta_r G(T)$ from the model predicts an 18% decrease in the FCWDS between 297 and 324 K, whereas the rate constant decreases by 45%. This implies a 40% decrease of $\langle|V|^2\rangle$ over this temperature range. The temperature dependence of k_{back} provides additional evidence of temperature dependent $|V|$ in mesitylene. The free energy change attending the back reaction (CS $\rightarrow$ S_1) is $+0.04$ eV at 297 K and reaches 0 eV near 330 K. Despite the increased driving force with increasing temperature, k_{back} decreases at temperatures above 314 K. As the FCWDS for k_{back} must increase from 297 to 330 K,[82] the only explanation for the decreasing rate constant is a decrease in $\langle|V|^2\rangle$.

The electron-transfer rate constants of **1** in 1,3-diisopropylbenzene (13DIP) display complicated temperature dependences; k_{for} and k_{back} both increase, plateau, and then decrease with increasing temperature. The solvation model does not reproduce the curvature of the $\Delta_r G(T)$ plot (see Figure 2), so the FCWDS-(*T*) were evaluated using the experimental $\Delta_r G(T)$ and the solvation model value of $\lambda_S(T)$. The FCWDS for the charge separation reaction (Figure 10) is relatively constant from 235 to 285 K and decreases by 300% from 285 to 345 K. The coupling, extracted from the $k_{for}(T)$ data, changes little between 235 and 285 K but drops more than 40% from 285 to 345 K.[83] The decrease of $|V|$ with temperature is comparable to that observed in mesitylene and is about twice as large as that observed in cumene. By contrast, the coupling for **1** in 1,3,5-triisopropylbenzene appears to increase with temperature. The data were obtained at lower temperatures, and over a limited range, because the charge separation reaction is endoergic at temperatures above 290 K. Both k_{for} and k_{back} increase from 260 to 290 K as $\Delta_r G(S_1 \rightarrow CS)$ increases from -0.02 to 0 eV. The increases of both rate constants can be achieved in two ways: (i) both reactions lie in the normal region and λ_o decreases very sharply over the 30 K range or (ii) the electronic coupling increases with temperature. The solvation model prediction, that λ_o decreases from 0.1 to 0.08 eV over this range, leads to less than a 5% change in the FCWDS. Thus, $|V|$ appears to increase with temperature.

The temperature dependence of solvent-mediated electronic coupling magnitude for **1** originates from a complex combination of configurational equilibria and electronic wave function overlap. Nonetheless, some general trends can be identified. For solvents that are not strongly influenced by steric constraints, increasing temperature leads to smaller observed couplings. This trend can be rationalized as reflecting an entropy driven[84] increase in the fraction of "empty" clefts at higher temperatures. For solvents with extreme steric bulk, the coupling increase with temperature. This may reflect enhanced population of "filled" cleft configurations, which provide larger couplings and are more accessible at higher temperatures.[84] From the data, it is evident that a variety of coupling versus temperature profiles are possible. The validity of these ensemble average interpretations could be assessed by performing more complete simulations of the electronic coupling magnitude, e.g., by a mixture of GMH calculations and molecular dynamics simulation that include contributions from solvent free clefts.[85]

Conclusions

The primary results of this body of work are the identification and characterization of solvent-mediated superexchange as a mechanism for electronic coupling between electron transfer donor and acceptor groups and the parametrization and evaluation of a molecular based model for the reaction free energy $\Delta_r G$ and solvent reorganization λ_o in polar and nondipolar solvents. The accurate implementation of the molecular solvation model is essential for the identification and quantification of electronic coupling magnitudes. From the form of eq 3, it is evident that assumed or inaccurate determinations of $\Delta_r G$ and λ_o significantly impact values of the electronic coupling extracted from rate constant measurements, because the former quantities appear in the argument of an exponential term and the latter appears in the preexponential factor. By careful experimental design that uses well-defined control studies and a rigorous implementation and parametrization of the solvation model, it is possible to achieve sufficient accuracy to identify solvent and temperature dependences for the electronic coupling and to extract electronic coupling magnitudes $|V|$.

Over the past six years, the analysis of the reaction free energy and solvent reorganization energy for these systems in different solvents has evolved from a simple continuum treatment to a molecular model that incorporates dipole, quadrupole, and dispersion interactions. The experimental measurement of reaction free energies for the electron-transfer reactions of **1** in the nondipolar and weakly polar solvents were critical to these

studies, because they allowed parametrization of the molecular solvation model. The most elaborate form of the solvation model suitably reproduces the reaction free energy and its temperature dependence for most of the solvents and makes reasonable predictions in the more polar solvents, for which the reaction free energy is not known experimentally. The deviation of the 2,5-dichlorotoluene results from the predictions underscores the fact that the model is not yet complete and should be enhanced, at least to include nonaxial charge distribution effects. The reliability of the model in predicting the solvent reorganization energy has proven difficult to assess. Further spectroscopic analyses of charge-transfer absorption and emission bands shapes as a function of temperature and solvent will be of use toward this end. Combinations of spectroscopic and kinetic studies, such as the work of Nelsen and co-workers,[86] should also prove to be of use in refining the molecular solvation model.

With access to reasonable FCWDS information, it becomes possible to analyze the electron-transfer rate data to expose the solvent and temperature dependence of the electronic coupling magnitude $|V|$. The observations in compounds **1** and **3** reveal a significant solvent dependence for the electronic coupling magnitude $|V|$. The value of $|V|$ depends on detailed aspects of the wave function overlap between the donor and acceptor orbitals and the mediating solvent orbitals, as revealed by a comparison of solvents that differ by their degree of alkyl substitution and size. In addition, the observed couplings for these systems correlate with the solvent molecule's vertical electron affinity, which is consistent with an electron-mediated superexchange interaction. The electronic couplings for **1** exhibit significant temperature dependence in some of the solvents. This dependence occurs because the experimental values reflect an ensemble averaging over solvent configurations within the cleft of the donor−spacer−acceptor molecule. This latter observation suggests that electron-transfer processes that involve solvent molecules may have strong non-Condon character; that is, the electronic coupling varies significantly with nuclear coordinates.

These findings suggest a number of important avenues for further study that will improve our understanding of electronic coupling and electron tunneling processes.

The important role that nuclear dynamics may play in solvent-mediated electronic coupling is an important avenue for future studies. The strong dependence of the electronic coupling on solvent position that is illustrated in Figures 6 and 7 provides good evidence that nuclear dynamics could play a role for electron tunneling processes which have nonbonded "steps" in their superexchange pathways. A need exists to identify reliable experimental signatures for such effects. In these studies, the temperature dependence of the coupling was assessed indirectly, from analysis of kinetic data necessitating accurate models for the FCWDS. It might be useful to investigate the solvent (vide infra) and temperature dependence of charge transfer absorption transitions whose intensity derives from solvent-mediated coupling, e.g., in highly curved ferrocene-spacer-ferrocinium molecules.

Although the correlation of the electronic coupling with the solvent molecule's electron affinity is significant, a number of important questions remain unanswered with respect to the energy gap dependence of the superexchange mechanism. For example, as the energy gap decreases, one expects an increase in the electronic coupling magnitude (for similar exchange interaction energies) and a transition to a new mechanism for the electron-transfer process. It may be that the transition to an adiabatic mechanism occurs and understanding the transition between regimes requires further study.[87] Alternatively, one may transition to a different mechanism in which the electron (or hole) hops between sites. These issues are central in understanding electron transfer for molecular systems with conjugated bridges and in biological systems, e.g., the primary steps in photosynthesis,[88] oxidation in DNA, and others. Well-defined studies that vary the energy gap and the number of sites between the donor and acceptor units can address these mechanistic issues.

The cleft molecules used in these studies only allow a single solvent molecule at a time on the "line-of-sight" between the donor and acceptor groups. The extent of coupling-mediated by more than one solvent is not addressed by these studies. Important dynamical and stereoelectronic considerations must be better understood in order for the distance dependence of electronic coupling via nonbonded contacts to be fully characterized.

The impact of solvent molecule location in the cleft site needs to be better addressed. Studies of the sort used by Napper et al.[89] show that location of the solvent in the line of sight is important; however, they do not probe the dynamics of solvent molecule's entering and leaving the cleft site. In the slow limit of conformational gating, one can see that a molecular binding event can be used as a trigger for electron transfer, and in the fast limit (**1** in benzene), the "cleft-bound" molecule is always present but accessing configurations with different coupling magnitudes. The transition from the "gated" limit to the thermal limit has not been probed and might display an interesting role for nuclear dynamics.

Determination of electronic coupling magnitudes from electron-transfer rate constants requires accurate values of $\Delta_r G$ and λ_o. Although a variety of solvation models predict these quantities, few experimental values are available, particularly of λ_o, for use in calibrating the models. The development of methods that allow direct measurements of these quantities, particularly in polar solvents, would be of great value.

Not only do these avenues represent interesting fundamental studies but their understanding will also be important for designing and manipulating electron processes in chemically and biologically important ways.

Acknowledgment. These studies were funded by the National Science Foundation (CHE-9206765, CHE-9708351, and CHE-0108945 to M. B. Z. and CHE-941693 and CHE-0111435 to D. H. W) and in part by the Department of Energy, Division of Chemical Sciences (DEFG02-89ER14062 to D. H. W.). We gratefully acknowledge discussions with Professors D. N. Beratan, R. Cave, K. D. Jordan, D. Matyushov, and M. Newton. These studies were completed by wonderful co-workers: H. Han, R. Kaplan, K. Kumar, Z. Lin, A. Napper, and I. Read. We thank Professor V. Fidler and Dr. P. Kapusta for measuring the low temperature charge transfer emission.

Supporting Information Available: A detailed presentation of the predicted reorganization energies for **1** in each of the solvents as a function of temperature, the different contributions to λ_o and $\Delta_r G$ at 295 K, and the solvent quadrupole and dipole properties are provided in tabular form. Plots of the electronic coupling as a function of solvent molecule displacement and angle are given for three additional cases. This material is available free of charge via the Internet at http://pubs.acs.org.

References and Notes

(1) (a) Closs, G. L.; Miller, J. R. *Science* **1988**, *240*, 440. (b) Paddon-Row, M. N. *Acc. Chem. Res.* **1994**, *27*, 18. (c) Barbara, P. F.; Meyer, T. J.; Ratner, M. A. *J. Phys. Chem.* **1996**, *100*, 13148.

(2) (a) Oevering, H.; Paddon-Row, M. N.; Heppener, M.; Oliver, A. M.; Costaris, E.; Verhoeven, J. W.; Hush, N. S. *J. Am. Chem. Soc.* **1987**, *109*, 3258. (b) Closs, G. L.; Calcaterra, L. T.; Green, N. J.; Penfield, K. W.; Miller, J. R. *J. Phys. Chem.* **1986**, *90*, 3673. (c) Helms, A.; Heiler, D.; McLendon, G. *J. Am. Chem. Soc.* **1992**, *114*, 6227. (d) Leland, B. A.; Joran, A. D.; Felker, P. M.; Hopfield, J. J.; Zewail, A. H.; Dervan, P. B. *J. Phys. Chem.* **1985**, *89*, 5571.

(3) (a) Helms, A.; Heiler, D.; McClendon G. *J. Am. Chem. Soc.* **1991**, *113*, 4325. (b) Sakata, Y.; Tsue, H.; O'Neil, M. P.; Wiederrecht, G. P.; Wasielewski, M. R. *J. Am. Chem. Soc.* **1994**, *116* (6), 6904. (c) Guldi, D. M.; Luo, C.; Prato, M.; Troisi, A.; Zerbetto, F.; Scheloske, M.; Dietel, E.; Bauer, W.; Hirsch, A. *J. Am. Chem. Soc.* **2001**, *123*, 9166.

(4) (a) Penfield, K. W.; Miller, J. R.; Paddon-Row, M. N.; Cotsaris, E.; Oliver, A. M.; Hush, N. S. *J. Am. Chem. Soc.* **1987**, *109*, 5063. (b) Stereochemical effects on electron transfer in complexes have been extensively investigated. See, for example: Pispisa, B.; Venanzi, M.; Palleschi, A. *J. Chem. Soc. Far. Trans.* **1994**, *90*, 435.

(5) (a) Finckh, P.; Heitele, H.; Volk, M.; Michel-Beyerle, M. E. *J. Phys. Chem.* **1988**, *92*, 6584. (b) Wasielewski, M. R.; Niemczyk, M. P.; Johnson, D. G.; Svec, W. A.; Minsek, D. W. *Tetrahedron* **1989**, *45*, 4785. (c) Zehnacker, A.; Lahmani, F.; Van Walree, C. A.; Jenneskens, L. W. *J. Phys. Chem. A.* **2000**, *104*, 1377.

(6) (a) Zusman, L. D *Z. Phys. Chem.* **1994**, *186*, 1. (b) Onuchic, J. N.; Beratan, D. N.; Hopfield, J. J. *J. Phys Chem.* **1986**, *90*, 3707.

(7) (a) Jortner, J. *J. Chem. Phys.* **1976**, *64*, 4860. (b) Bixon, M.; Jortner, J. *Adv. Chem. Phys.* **1999**, *106*, 35.

(8) (a) Kelley, A. M. *J. Phys. Chem. A* **1999**, *103*, 6891. (b) Spears, K. G.; Wen, X.; Zhang, R. *J. Phys. Chem.* **1996**, *100*, 10206. (c) Wang, C.; Mohney, B. K.; Williams, R.; Hupp, J. T.; Walker, G. C. *J. Am. Chem. Soc.* **1998**, *120*, 5848. (d) Markel, F.; Ferris, N. S.; Gould, I. R.; Myers, A. B. *J. Am. Chem. Soc.* **1992**, *114*, 6208.

(9) (a) The charge-separated state has been observed via charge-transfer fluorescence from shorter spacer systems[15] and by transient absorbance of the anthracene radical cation in **1**.[9b] (b) N. Segal, Undergraduate Thesis, Brown University, Providence, RI.

(10) Corroborating evidence for equilibrium between the locally excited and charge transfer states of **1** in benzene was obtained from transient absorption spectroscopy.[9b] The formation and decay rate constants of the anthracene radical cation are the same as the two rate constants observed using time-resolved fluorescence spectroscopy.

(11) Gu, Y.; Kumar, K.; Lin, Z.; Read, I.; Zimmt, M. B.; Waldeck, D. H. *J. Photochem. Photobiol. A.* **1997**, *105*, 189.

(12) Read, I.; Napper, A.; Kaplan, R.; Zimmt, M. B.; Waldeck, D. H. *J. Am. Chem. Soc.* **1999**, *121*, 10976.

(13) The recombination rate process involves an unknown partitioning to form the ground singlet state, S_0, and to form the lowest triplet state, T_1.

(14) (a) Marcus, R. A. *J. Phys. Chem.* **1989**, *93*, 3078. (b) Cortes, J.; Heitele, H.; Jortner, J. *J. Phys. Chem.* **1994**, *98*, 2527. (c) Matyushov, D. V.; Newton, M. D. *J. Phys. Chem. A* **2001**, *105*, 8516. (d) Hush, N. S. *Prog. Inorg. Chem.* **1967**, *8*, 391.

(15) (a) Zeng, Y.; Zimmt, M. B. *J. Phys. Chem.* **1992**, *96*, 8395. (b) Zeng, Y.; Zimmt, M. B. *J. Am. Chem. Soc.* **1991**, *113*, 5107.

(16) Kumar, K.; Kurnikov, I.; Beratan, D. N.; Waldeck, D. H.; Zimmt, M. B. *J. Phys. Chem. A* **1998**, *102*, 5529.

(17) (a) Sitkoff, D.; Sharp, K. A.; Honig, B. *J. Phys. Chem.* **1994**, *98*, 1978. (b) Sharp, K.; Honig, B. *Annu. Rev. Biophys. Biophys. Chem.* **1990**, *19*, 301. (c) Newton, M. D.; Basilevsky, M. V.; Rostov, I. V. *Chem. Phys.* **1998**, *232*, 201.

(18) (a) Jeon, J.; Kim, H. J. *J. Phys. Chem. A* **2000**, *104*, 9812. (b) Dorairaj, S.; Kim. H. J. *J. Phys. Chem. A* **2002**, *106*, 2322.

(19) Matyushov, D. V.; Voth, G. A. *J. Chem. Phys.* **1999**, *111*, 3630.

(20) Read, I.; Napper, A.; Zimmt, M. B.; Waldeck, D. H. *J. Phys. Chem. A* **2000**, *104*, 9385.

(21) Napper, A. M.; Read, I.; Kaplan, R.; Zimmt, M. B.; Waldeck, D. H. *J. Phys. Chem. A* **2002**, *106*, 5288.

(22) Napper, A. M.; Read, I.; Waldeck, D. H.; Kaplan, R. W.; Zimmt, M. B.; *J. Phys. Chem. A* **2002**, *106*, 4784.

(23) Brunschwig, B. S.; Ehrenson, S.; Sutin, N. *J. Phys. Chem.* **1986**, *90*, 3657.

(24) (a) Peng, B.-C.; Newton, M. D.; Raineri, F. O.; Friedman, H. L. *J. Chem. Phys.* **1996**, *104*, 7153. (b) Peng, B.-C.; Newton, M. D.; Raineri, F. O.; Friedman, H. L. *J. Chem. Phys.* **1996**, *104*, 7177.

(25) Although initial results are encouraging, whether the inclusion of quadrupolar responses is successful at extending continuum treatments to nonpolar and weakly polar solvents remains an open question.[18]

(26) (a) Vath, P.; Zimmt, M. B.; Matyushov, D. V.; Voth, G. A. *J. Phys. Chem. B* **1999**, *103*, 9130. (b) Vath, P.; Zimmt, M. B. *J. Phys. Chem. A* **2000**, *104*, 2626.

(27) Gray, C. G.; Gubbins, K. E. *Theory of Molecular Fluids, Vol. 1*; Clarendon Press: Oxford, 1984.

(28) (a) Matyushov, D. V.; Schmid, R. *J. Chem. Phys.* **1996**, *104*, 8627. (b) Ben-Amotz, D.; Herschbach, D. R. *J. Phys. Chem.* **1990**, *94*, 1038.

(29) Kumar, K. PhD Thesis, Brown University, Providence, RI, 1996.

(30) This difference in polarizabilities is given more explicitly in refs 20 and 21.

(31) The molecular solvation model assumes that the quadrupole is axial with its major axis along the dipole moment direction. Table S1 in the Supporting Information shows that the quadrupole moments in 2,5-dichlorotoluene and many of the alkylbenzenes are nonaxial; that is, the major axis of the quadrupole moment's principal axis system is not oriented along the dipole moment vectors direction and the other components of the quadrupole moment tensor are not equal in magnitude.

(32) Gubbins, K. E.; Gray, C. G.; Machado, J. R. S. *Mol. Phys.* **1981**, *42*, 817.

(33) To assess whether the nonaxial part of the quadrupole could be used to correct the electrostatic interactions in a way that is qualitatively correct, the model was implemented with an effective quadrupole moment, given by $Q_{\text{eff}} = \langle Q \rangle - b\langle Q_{\text{nonaxial}} \rangle$ with b an adjustable parameter.

(34) An alternative approach would be to use best fit values for the continuum model, they are $\Delta_{\text{vac}}G = 0.295$ eV, and a radius $= 7.8$ Å.

(35) A detailed presentation of the predicted reorganization energies for **1** in each of the solvents as a function of temperature is provided in the Supporting Information.

(36) (a) Eigler, D. M.; Lutz, C. P.; Rudge, W. E. *Nature (London)* **1991**, *352*, 600.

(37) (a) Segal, D.; Nitzan, A.; Ratner, M.; Davis, W. B. *J. Phys. Chem. B* **2000**, *104*, 2790. (b) Sumi, H.; Kakitani, T. *J. Phys. Chem. B.* **2001**, *105*, 9603. (c) Felts, A. K.; Pollard. W. T.; Friesner, R. A. *J. Phys. Chem.* **1995**, *99*, 2929.

(38) Halpern, J.; Orgel, L. E. *Discuss. Faraday. Soc.* **1960**, *29*, 32.

(39) McConnell, H. M. *J. Chem. Phys.* **1961**, *35*, 508.

(40) (a) Evenson, J. W.; Karplus, M. D. *Science* **1993**, *262*, 1247. (b) Paddon-Row, M. N.; Shephard, M. J.; Jordan, K. D. *J. Am. Chem. Soc.* **1993**, *115*, 3312. (c) Larsson, S. *J. Am. Chem. Soc.* **1981**, *103*, 4034.

(41) (a) Newton, M. D. *Chem. Rev.* **1991**, *91*, 767. b) Jordan, K. D.; Paddon-Row, M. N. *Chem. Rev.* **1992**, *92*, 295.

(42) (a) Liang, C.; Newton, M. D. *J. Phys. Chem.* **1993**, *97*, 3199. (b) Jortner, J.; Bixon, M.; Voityuk, A. A.; Roesch, N. *J. Phys. Chem. A* **2002**, *106*, 7599. (c) Sikes, H. D.; Smalley, J. F.; Dudek, S. P.; Cook, A. R.; Newton, M. D.; Chidsey, C. E. D.; Feldberg, S. W. *Science* **2001**, *291*, 1519. (d) Winkler, J. R.; Gray, H. B. *J. Biol. Inorg. Chem.* **1997**, *2*, 399.

(43) Beratan, D. N.; Onuchic, J. N. *Photosyn. Res.* **1989**, *22*, 173.

(44) (a) Balabin, I. A.; Onuchic, J. N. *J. Phys. Chem.* **1996**, *100*, 11573. (b) Naleway; C. A.; Curtiss, L. A.; Miller, J. R. *J. Phys. Chem.* **1991**, *95*, 8434. (c) Ratner, M. D. *J. Phys. Chem.* **1990**, *94*, 4877.

(45) (a) Miller, J. R.; Beitz, J. V.; Huddleston, R. K. *J. Am. Chem. Soc.* **1984**, *106*, 5057. (b) Launay, J.-P. *Chem. Soc. Rev.* **2001**, *30*, 386. (c) Fernando, S. R. L.; Kozlov, G. V.; Ogawa, M. Y. *Inorg. Chem.* **1998**, *37*, 1900. (d) See also refs 1 and 2.

(46) Recent experimental and theoretical studies indicate alternatives to superexchange type mechanisms for long distance electron transfer. The fall off of transfer rates with distance by these mechanisms is much weaker than for superexchange mechanisms. See refs 37 and 41.

(47) Tong, G. S. M.; Kurnikov, I. V.; Beratan D. N. *J. Phys. Chem. B*, **2002**, *106*, 2381. Benrahmoune, M.; Filali-Mouhim, A.; Jay-Gerin, J.-P. *Can. J. Phys. Pharm.* **2001**, *79*, 122.

(48) Beratan, D. N.; Hopfield, J. J. *J. Am. Chem. Soc.* **1984** *106*, 1584.

(49) Beratan, D. N. *J. Am. Chem. Soc.* **1986**, *108*, 4321.

(50) Reed, A. E.; Curtiss, L. A.; Weinhold, F. *Chem. Rev.* **1988**, *88*, 899.

(51) Petrov, E. G.; Zelinsky, Y. R.; May, V. *J. Phys. Chem.* **2002**, *106*, 3092.

(52) (a) Davis W. B.; Ratner, M. A.; Wasielewski, M. R. *Chem. Phys.* **2002**, *281*, 333. (b) Giese B *Annu. Rev. Biochem.* **2002**, *71*, 51.

(53) (a) Osuka, A.; Maruyama, K.; Mataga, N.; Asahi, T.; Yamazaki, I.; Tamai, N. *J. Am. Chem. Soc.* **1990**, *112*, 4958. (b) McLendon, G.; Helms, A.; Heiler, D. *J. Am. Chem. Soc.* **1992**, *114*, 6227. (c) Kang, Y. K.; Rubtsov, I. V.; Iovine, P. M.; Chen, J.; Therien, M. J. *J. Am. Chem. Soc.* **2002**, *124*, ASAP.

(54) See also: Miller, S. E.; Marsh, E. M.; Svec, W. A.; Debreczeny, M. P.; Wasielewski, M. R. *Book of Abstracts, 216th ACS National Meeting*, Boston, 1998, PHYS-132.

(55) Tsue, H.; Imahori, H.; Kaneda, T.; Tanaka, Y.; Okada, T.; Tamaki, K.; Sakata, Y. *J. Am. Chem. Soc.* **2000**, *122*, 2279.

(56) Miller, J. R. *New J. Chem.* **1987**, *11*, 83.

(57) (a) Balabin, I. A.; Onuchic, J. N. *Science* **2000**, *290*, 114. (b) Xie, Q.; Archontis, G.; Skourtis, S. S. *Chem. Phys. Lett.* **1999**, *312*, 237. (c) Medvedev, E. S.; Stuchebrukhov, A. A. *J. Chem. Phys.* **1997**, *107*, 3821. (d) Tang, J. *J. Chem. Phys.* **1993**, *98*, 6263. (e) Hoffman, B. M.; Ratner, M. A.; Wallin, S. A. *Adv. Chem. Ser.* **1990**, *226*, 125. (f) Xu, Q.; Baciou, L.; Sebban, P.; Gunner, M. R. *Biochemistry* **2002**, *41*, 10021.

(58) (a) Carapelluci, P. A.; Mauzerall, D. *Ann. NY. Acad. Sci. B* **1975**, *244*, 214. (b) Ballard, S. G.; Mauzerall, D. *Tunneling Biol. Syst. [Proc. Symp.]* **1979**, 581; Chance, B., Marcus, R. A., DeVault, D. C., Eds.

(59) Oliver, A. M.; Craig, D. C.; Paddon-Row, M. N.; Kroon, J.; Verhoeven, J. W. *Chem. Phys. Lett.* **1988**, *150*, 366.

(60) Liu, J.-Y.; Schmidt, J. A.; Bolton, J. R. *J. Phys. Chem.* **1991**, *95*, 6924.

(61) (a) Ojima, S.; Miyasaka, H.; Mataga, N. *J. Phys. Chem.* **1990**, *94*, 7534. (b) Yabe, T.; Kochi, J. K. *J. Am. Chem. Soc.* **1992**, *114*, 4491.

(62) (a) Lawson, J. M.; Paddon-Row, M. N.; Schuddeboom, W.; Warman, J. M.; Clayton, A. H. A.; Ghiggino, K. P. *J. Phys. Chem.* **1993**, *97*, 13099. (b) Seischab, M.; Lodenkemper, T.; Stockmann, A.; Schneider, S.; Koeberg, M.; Roest, M. R.; Verhoeven, J. W.; Lawson, J. M.; Paddon-Row, M. N. *Phys. Chem. Chem. Phys*. **2000**, *2*, 1889.

(63) Gould, I. R.; Mueller, L. J.; Farid, S. *Zeit. Phys. Chem. N. F.* **1991**, *170*, 143.

(64) (a) Head, N. J.; Oliver, A. M.; Look, K.; Lokan, N. R.; Jones, G. A.; Paddon-Row, M. N. *Angew Chem. Int. Ed.* **1999**, *38*, 3219. (b) Prigge, S. T.; Kolhekar, A. S.; Eipper, B. A.; Mains, R. E.; Amzel, L. M. *Nature. Struct. Biol.* **1999**, *6*, 976.

(65) β in a vacuum is ~2.7 Å. See: Henderson, T. M.; Cave, R. J. *J. Chem. Phys.* **1998**, *109*, 7414.

(66) Lokan, N. R.; Paddon-Row, M. N.; Koeberg, M.; Verhoeven, J. W. *J. Am. Chem. Soc.* **2000**, *122*, 5075.

(67) (a) Verhoeven, J. W. *Adv. Chem. Phys.* **1999**, *106*, 603. (b) Cave, R. J.; Newton, M. D.; Kumar, K.; Zimmt, M. B. *J. Phys. Chem.* **1995**, *99*, 17501.

(68) (a) Cave, R. J.; Newton, M. D. *Chem Phys Lett* **1996**, *249*, 15. (b) Cave, R. J.; Newton, M. D. *J. Chem. Phys.* **1997**, *106*, 9213.

(69) (a) There are systems where through bond coupling may exhibit significant fluctuations because of small structural changes. This includes electron-transfer systems involving conformational gating, structural fluctuations of proteins[57] and symmetry breaking.[15,69b,c] (b) Jones, G. A.; Paddon-Row, M. N.; Carpenter, B. K.; Piotrowiak, P. *J. Phys. Chem. A.* **2002**, *106*, 5011. c) Reimers, J. R.; Hush, N. S. *Chem. Phys*. **1990**, *146*, 105.

(70) (a) This expression was derived from a thermodynamic cycle that transfers the transition state to the gas phase, separates the D*SA and solvent to infinity, performs the vertical electron transfer, brings the ions together in the same geometry of the reactants, and solvates the resulting species by the solvent polarization needed to achieve the transition state. According to Matyushov,[70b] this solvent polarization may be expressed as $P_{TS} = (\Delta_r G + \lambda_S)/(\mu_{CT} - \mu_{S1})$ and that $\Delta_{TS\_SOLV} = -(\Delta_r G + \lambda_S) * (\mu_{D+S-A} - \mu_{S1})/(\mu_{CT} - \mu_{S1})$. (b) Milischuk, A.; Matyushov, D. V, submitted.

(71) The Coulomb term will vary if the separations of D+ and S− change drastically with solvent. The fourth term varies insignificantly with solvent dielectric properties.[70]

(72) These calculations used a nonsymmetric conformation of the spacer and acceptor ester groups to avoid rigorous (mathematical) symmetry constraints on the coupling.

(73) The scaling equation used is $EA_V = -0.9093E(6\text{-}31G^{**}) + 2.507$, with all values in eV.

(74) Kaplan, R.; Napper, A. M.; Waldeck, D. H.; Zimmt, M. B. *J. Phys. Chem. A.* **2002**, *106*, 1917.

(75) The 40-fold drop is premised on a through space decrease of wave function overlap and exchange arising from a β value of -2.6/Å.[65,66]

(76) The small decrease of $(T_{D^*S}\ T_{SA})^{1/2}$ from **1** to **3** may reflect, in part, the change from symmetry forbidden donor−acceptor topology in **1** to a symmetry allowed donor−acceptor topology in **3**. As most in-cleft solvent configurations for both molecules are dissymmetric, the symmetry forbidden nature of the donor−acceptor interaction for **1** should not be heavily expressed in the donor-spacer and spacer-acceptor interactions.

(77) β for the 7.5 and 9.5 Å U-shaped molecules was estimated using rate constants extracted from Figure 3B in ref 66. To one significant figure, the β values are 1 (in TIP, benzene, o-dichlorobenzene, acetonitrile), 0.8 (ethyl acetate), 0.4 (benzylcyanide, tetrahydrofuran), and 0.3(dibutyl ether, diethyl ether).

(78) One additional point is worth making regarding the role of spacer structure. Our initial investigations of solvent-mediated coupling employed three highly curved molecules, **1**, **4**, and **5**, with charge separation distances of 7.1, 10.2, and 10.6 Å, respectively. Although the $|V|$ for **5** was 7 times smaller than for **1** in both acetonitrile and benzonitrile ($\beta \sim 1.1$ Å^{-1}), $|V|$ for the shorter separation in **4** was 9.4 times smaller than for **1** in benzonitrile ($\beta \sim 1.4$ Å^{-1}). Inspection of the CPK model for **4** reveals that a spacer norbornyl CH_2 group that is proximal to the acceptor lies close to the "bird's eye path" from the donor to the acceptor. This CH_2 group eliminates a set of solvent configurations that otherwise might establish significant exchange interactions with both the donor and the acceptor. For the purposes of investigating the distance dependence of solvent-mediated coupling, this spacer is inadequate.

(79) A molecular mechanics calculation was performed on each of the 78 configurations of benzene within the cleft of **1**. These energies were used to calculate the relative probability of each configuration.

(80) This results from the symmetry forbidden topology that causes the average electronic coupling to be near zero. For a system in which the direct interaction was symmetry allowed, the average value would be more comparable to the root-mean-square value.

(81) The rate constants for **1** in mesitylene exhibit similar variations with temperatures but have been measured over a smaller temperature range.

(82) Because $\Delta_r G$ attending k_{back} is positive between 297 and 330 K, this electron-transfer step must lie in the normal region. Consequently, the FCWDS must increase from 297 to 330 K as $\Delta_r G$ decreases from +0.04 eV to 0.0 eV.

(83) The solvation model underestimates the increase in $\Delta_r G$ at high temperatures. Based on correlations observed between $d(\Delta_r G)/dT$ and $d(\lambda_o)/dT$, this implies that the actual slope of $d(\lambda_o)/dT$ is more negative than predicted by the solvation model and that the solvation model estimates of λ_o above 315 K are slightly too large. Because the charge separation event lies in the normal region ($\Delta_r G > 0$ eV), the calculated FCWDS are too large. This implies that the actual decrease in $|V|$ at temperatures above 315 K will be steeper than indicated in the present analysis.

(84) Formation of a DSA−solvent "complex" is likely attended by a decrease in entropy. For aromatic solvents with small or no alkyl groups, ΔH for formation of this complex may be negative or close to zero. For aromatic solvents with bulky alkyl groups, ΔH for complex formation will be more positive.

(85) (a) Castner, E. W.; Kennedy, D.; Cave, R. J. *J. Phys. Chem. A* **2000**, *104*, 2869. (b) Troisi, A.; Ratner, M., manuscript in preparation.

(86) Nelsen, S. F.; Ismagilov, R. F.; Gentile, K. E.; Powell, D. R. *J. Am. Chem. Soc.* **1999**, *121*, 7108.

(87) (a) Khoshtariya, D. E.; Dolidze, T. D.; Zusman, L. D.; Waldeck, D. H. *J. Phys. Chem. A.* **2001**, *105*, 1818. (b) Weaver, M. J. *Chem. Rev.* **1992**, *92*, 463.

(88) (a) Diner, B. A.; Rappaport, F. *Annu. Rev. Plant Biol.* **2002**, *53*, 551. (b) Hoff, A. J.; Deisenhofer, *J. Phys. Rep*. **1997**, *287*, 1. (c) Ivashin, N.; Larsson, S. *J. Phys. Chem. B* **2002**, *106*, 3996.

(89) (a) Napper, A. M.; Head, N. J.; Oliver, A. M.; Shephard, M. J.; Paddon-Row, M. N.; Read, I.; Waldeck, D. H *J. Am. Chem. Soc.* **2002**, *124*, 10171. (b) Napper, A. M.; Read, I.; Waldeck, D. H.; Head, N. J.; Oliver, A. M.; Paddon-Row, M. N. *J. Am. Chem. Soc.* **2000**, *122*, 5220.

(90) Fidler, V.; Kapusta, P., personal communication.